

**FINAL REPORT**

**Topic No: N98-142**

***Low Cost Grating Based Laser Sensor***

**For Contract Period:  
October 8, 1998 through April 15, 1999**

**Contract No: N00014-99-M-0008**

**Submitted to:**

**OFFICE OF NAVAL RESEARCH**

**Attn: John Thomas  
800 North Quincy Street  
Arlington, VA 22217-5660**

**Submitted by:**

**OPTRA, Inc.  
461 Boston Street  
Topsfield, MA 01983**

**Principal Investigator: Craig Schwarze**

**Phone: (978) 887-6600 x125**

**E-Mail: [cschwarz@optra.com](mailto:cschwarz@optra.com)**

**This report is Unclassified**

**19990426 034**

**DTIC QUALITY INSPECTED 2**

**DISTRIBUTION STATEMENT A  
Approved for Public Release  
Distribution Unlimited**

**OPTRA**

## Table of Contents

1.0	Identification and Significance of the Opportunity .....	2
2.0	Program Objectives and Phase I Approach .....	3
3.0	Work Completed during Phase I R&D .....	4
3.1	Grating Analysis .....	5
3.1.1	Grating Experimental Results.....	9
3.2	Radiometry Analysis .....	12
3.2.1	Radiometry experimental data.....	14
3.3	Image Sensor Research .....	16
3.3.1	CCD Image Sensors .....	17
3.3.2	CMOS Image Sensor.....	19
3.3.3	Image Sensor Data.....	20
3.4	Cosmic Ray Research .....	23
3.5	Pulsed Laser Detection Electronics .....	23
3.5.1	Pulsed Laser Electronics Breadboard Testing.....	24
3.6	Algorithm Development .....	27
3.6.1	Algorithm experimental results.....	28
4.0	Conclusions .....	31
5.0	Recommendations .....	32

## Low Cost, Grating Based Laser Warning Sensor

Final Report Draft

March 19, 1999

### 1.0 Identification and Significance of the Opportunity

This research is being done in response to the current threat that lasers pose to pilots and other flight personnel. Visible and near infrared lasers can cause significant loss of visual function due to the high susceptibility of the eye to damage by laser radiation, particularly since the eye focuses all of the collected light from a well-collimated laser beam into a small spot on the retina. This damage is even greater when binoculars or similar devices are used, since the amount of collected light is greatly increased while the spot size remains the same. The end result is that even relatively low power lasers can temporarily or permanently impair vision from ranges of tens of miles or more. The widespread commercial availability of such lasers, at a variety of wavelengths in the visible and near IR, makes this an even more serious threat.

The damage to the eye resulting from laser radiation varies from temporary visual impairment (e.g. flash blindness) to permanent vision damage and blindness, depending on the laser power level and exposure duration. Even if the visual impairment is not permanent, a momentary distraction to a pilot can have severe consequences.

The goal of this program is the development of a laser sensor that warns of the presence of a potentially harmful level of laser illumination, and records pertinent event information (laser power, wavelength, pulse duration, pulse repetition frequency, time of exposure, and an image of the scene containing the threat). Such a sensor will not only protect flight personnel from unknowing exposure, but will also generate a database of such laser exposures. This database will be a valuable tool in the development of protective devices and suitable countermeasures. A technically competent Laser Warning Sensor that meets our target cost goal of  $\leq \$500$  will be inexpensive enough to be installed in a large number of Naval aircraft, thus affording widespread protection to aircrews, and assuring the generation of a meaningful database.

## 2.0 Program Objectives and Phase I Approach

The primary objective for this program is to develop a laser sensor for the measurement of laser illumination events during flight. The proposed sensor consists of a diffraction grating, CCD array, fast photodiode, and signal-processing electronics, which perform event extraction and recording. The target requirements are to measure the wavelength, average power, pulse length, pulse repetition frequency, and duration for each event and save the information in a time-stamped downloadable format. The sensor will run off its own power, be compact in size, and will mount to the interior windscreen of the aircraft. Furthermore, the final product will use commercial off-the-shelf parts in order to realize a cost to the consumer of less than \$500.00.

The target requirements for the sensor are given in the following table.

Item	Specification
Wavelength Range	0.4 – 1.1 $\mu\text{m}$
Wavelength Resolution	$\leq 10 \text{ nm}$
Field of View	$\geq 30 \text{ deg}$
Dynamic Range	$\geq 5000:1$
Minimum Detectable Pulse Length	$\leq 10 \text{ ns}$
Operating Lifetime	$\geq 6 \text{ hours}$
Event Recording	<ul style="list-style-type: none"><li>- Wavelength</li><li>- Average power</li><li>- Pulse length</li><li>- Pulse repetition frequency</li><li>- Duration</li><li>- IRIG Time Stamp</li></ul>
Data Update Rate	$\geq 100 \text{ Hz}$
Data Storage	$\geq 4 \text{ hour mission}$
Size	Handheld
Weight	$\leq 1/2 \text{ lb}$
Market Price	$\leq \$500.00$

Table 1. Low-cost Laser Warning Sensor target requirements

The objective of the Phase I research was to demonstrate the feasibility and practicality of a low-cost diffraction grating laser-warning sensor based on the proposed design. This objective was accomplished by performing the following technical objectives:

1. Develop a diffraction grating analytical model for use in designing an optimum grating for wavelength range, resolution, dynamic range, and sensor field-of-view.
2. Perform a radiometry analysis to determine the detection threshold and required dynamic range to measure laser illumination levels from glare to maximum permissible exposure.
3. Research and assess the current capability of CCD and CMOS array sensors in terms of performance (e.g. pixel size, wavelength responsivity range, dead zones, etc.), ease of

electronic integration and control (i.e. commercial off-the-shelf electronics, versus homegrown electronics design), software requirements, and cost.

4. Procure the major elements of the system and perform breadboard testing to verify the ability to measure and extract laser illumination information (e.g. wavelength, power, resolution, and dynamic range).
5. Design, breadboard, and verify the ability to measure pulsed laser event information (e.g. pulse length, duty cycle, and pulse repetition frequency)
6. Develop digital image processing algorithms for extracting wavelength and source irradiance (power) information from images of scenes containing laser sources.

All of these objectives were successfully accomplished during the course of the Phase I effort, thus demonstrating the feasibility of this technique. Optra believes these results clearly indicate the ability to design a low-cost laser warning sensor that satisfies all the requirements in Table 1.

### 3.0 Work Completed during Phase I R&D

Figure 1 shows a schematic of the laser warning sensor design. The measurement of a laser illumination event is provided by two separate subassemblies; 1) the grating/CCD pair is used to measure the wavelength, average power, and event duration, and 2) the fast photodiode is used to measure pulse length and pulse repetition frequency (PRF).

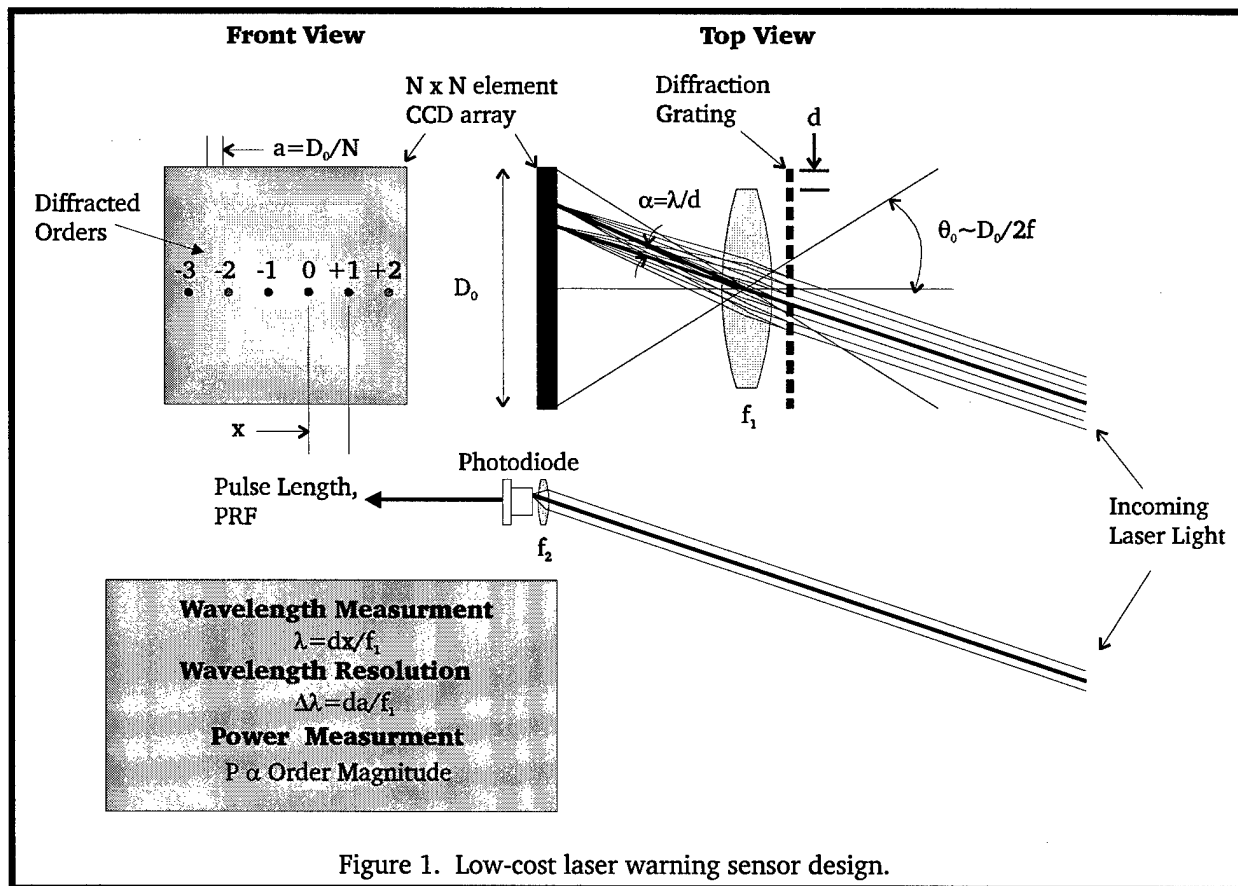


Figure 1. Low-cost laser warning sensor design.

Laser light that illuminates the sensor is diffracted by the grating into specific orders that are separated in angle an amount given by laser wavelength. These orders are focused onto the CCD

array, where they are detected, readout, and processed to determine their relative separation. The laser wavelength is determined using the measured separation and geometry. The laser power is determined from the magnitude of the diffracted orders; this magnitude is strictly a function of the grating parameters (e.g. pitch, aperture, etc.) – thus once the grating design is defined, the power is related to the order magnitude via a constant.

The field of coverage (FOC) is a cone that subtends an angle given by the focal length of the focusing lens,  $f_1$ , and the aperture of the CCD array,  $D_0$ ,

$$FOC \sim 2\theta_0 \sim D_0/f_1. \quad (1)$$

The grating will diffract a portion of the light from a laser source within the FOC at angles,

$$\alpha = n\lambda/d, \quad (2)$$

where  $d$  is the pitch of the grating and  $n$  is the order number. The lens focuses the diffracted orders from the grating onto the CCD array as shown in the left-hand portion of the figure, with the resulting spots separated by an amount,

$$x = f_1\alpha = f_1\lambda/d. \quad (3)$$

The wavelength is then determined by solving for  $x$  to obtain,

$$\lambda = \frac{xd}{f_1}. \quad (4)$$

Also, the wavelength resolution is given by the pixel size of the CCD array,

$$\Delta\lambda_{\min} = \frac{\Delta x_{\min} d}{f_1} = \frac{ad}{f_1}. \quad (5)$$

Since commercial CCD arrays work at TV frame rates (e.g. 30 Hz), a fast photodiode is used to measure the temporal characteristics of a pulsed input waveform. The field of coverage for the photodiode is given by the size of the active area of the detector,  $D_1$ , and the focal length of the collection lens,  $f_2$ , and is set as big as the wavelength field of coverage,

$$FOC_d = D_1/f_2 = D_0/f_1 \quad (6)$$

The following sections provide a detailed summary of the design and analysis performed during the Phase I R&D effort.

### 3.1 Grating Analysis

A diffraction grating is an optical device that exhibits a periodically varying refractive index or thickness that modulates the phase of the light passing through it<sup>1</sup>. As a result of this phase modulation, the light exiting the grating mixes and creates regions of constructive interference at angles,

$$\theta_q = \theta_i + n\lambda/d, \quad (7)$$

---

<sup>1</sup> Fundamentals of Photonics, B.E.A Saleh and M.C. Teich, John Wiley and Sons, NY, 1991

where  $d$  is the grating period, or pitch of the grating,  $n$  is the order number,  $\theta_i$  is the incident angle, and  $\theta_d$  is the diffracted angle. Note that light at different wavelengths will be diffracted along different directions, which allows for the unique determination of the incoming laser wavelength.

In the case of Fraunhofer diffraction (i.e. the diffraction pattern obtained at infinity, which is the case for the proposed system since a lens is used to focus the orders onto the CCD array) it can be shown that the field strength is obtained from the Fourier transform<sup>2</sup>,

$$E(p) = E_0 \int_{-\infty}^{\infty} A(x) e^{j2\pi p x} dx \quad (8)$$

where  $A(x)$  is the aperture function and  $p$  is the conjugate variable,

$$p = \sin \theta / \lambda. \quad (9)$$

Thus, once the aperture function is known, the Fourier transform can be taken to yield the amplitude distribution of the diffraction pattern in the far field.

The most common type of diffraction grating is a piece of glass lined with rulings. For this case, the aperture function can be written as,

$$A(x) = \Pi_{Nd}(x) [\Pi_a(x) * III_d(x)] \quad (10)$$

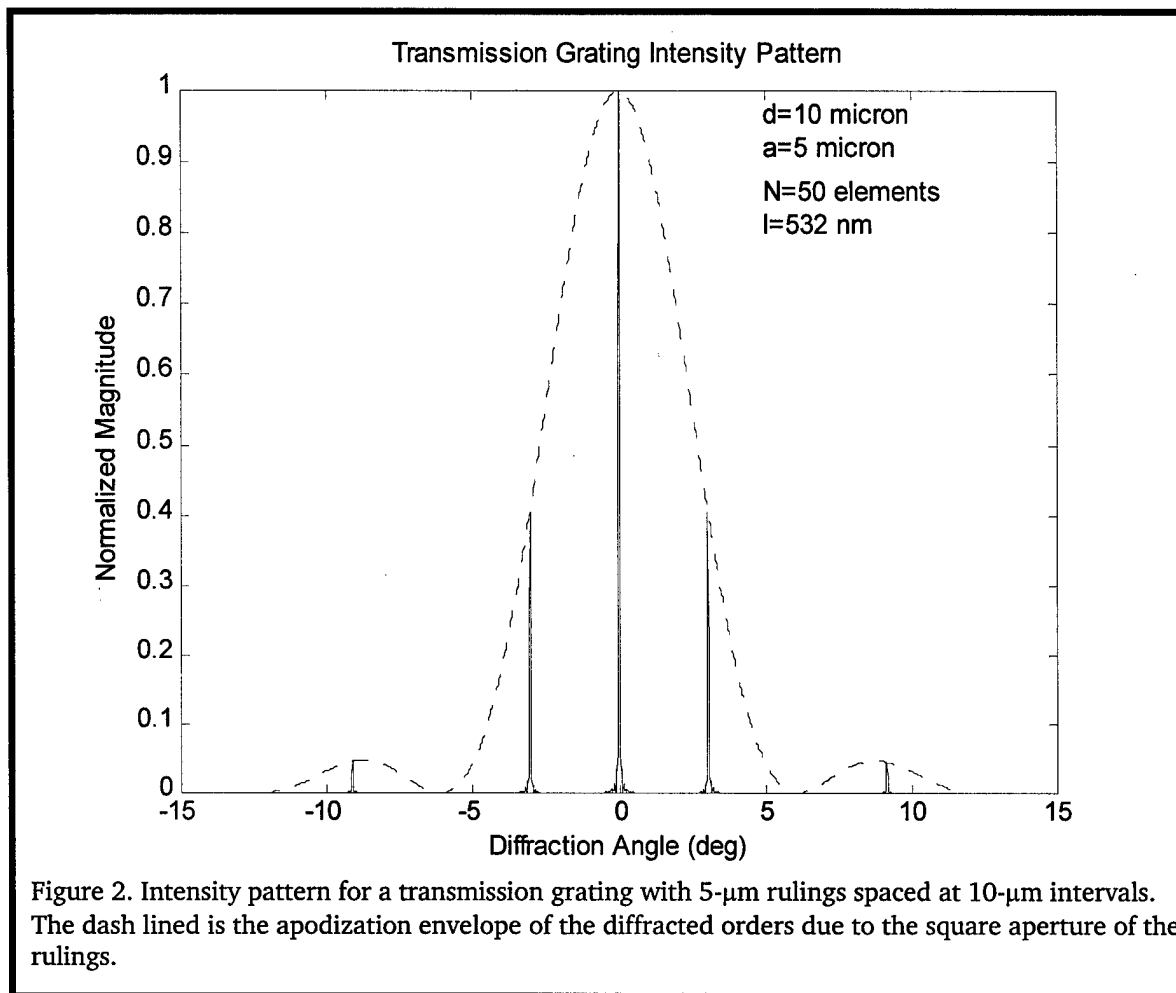
where  $N$  is the number of elements,  $d$  is the grating pitch, and  $a$  is the slit width. The function in Equation 10 describes a Dirac Comb ( $III_d(x)$ ) with spacing  $d$  that is convolved with a pulse ( $\Pi_a(x)$ ) of width  $a$ , and then apodized by a pulse ( $\Pi_{Nd}(x)$ ) of width  $Nd$ . Taking the Fourier transform of Equation 10 and using the convolution theorem (which states that the operation of convolution is the same as multiplication in the Fourier domain, and vice versa) gives the field diffraction amplitude as,

$$E(\theta) = E_0 \text{sinc}(\pi Nd \sin \theta / \lambda) * \left[ \text{sinc}(\pi a \sin \theta / \lambda) III_{\lambda/d}(\sin \theta / \lambda) \right] \quad (11)$$

where the sinc-function is the  $\sin(x)/x$  function. The second factor in Equation 11 is another Dirac comb with spacing  $\lambda/d$  multiplied by a very broad sinc-function (because  $a$  is very small), which is then convolved with a very narrow sinc-function (since  $Nd$  is very large). Figure 2 illustrates the intensity diffraction pattern (the intensity is effectively the square of the field amplitude) obtained in Equation 11 for a 10- $\mu\text{m}$  pitch grating with a 50% duty cycle (i.e. the slit width is 5- $\mu\text{m}$ ) at a wavelength of 532 nm. The data obtained for the figure was obtained from a MATLAB model that was developed during the course of the Phase I research effort.

---

<sup>2</sup> A student's guide to Fourier transforms with applications in physics and engineering, J.F. James, Cambridge University Press, NY, 1995



Some key observations from Figure 2 are the following:

1. The orders are equally spaced; this result allows the wavelength to be uniquely determined from any two orders, thus maximizing the angular field of coverage. For instance, if laser illumination is incident at an angle such that the +1 and higher positive orders fall off the detector, the wavelength can still be determined from 0 and -1 order.
2. As the number of slits becomes big, the width of each order becomes narrower; ultimately, for a very reasonable number of slits (e.g.  $\geq 20$ ) the width of the order will be determined by the diffraction limit of the optics used to focus the orders. This is a good result for the laser warning sensor since the grating can be designed so as not to limit the resolution of the system.
3. The diffracted orders are apodized by the Fourier transform of the aperture, which results in different magnitudes for the diffracted orders. However, since energy is necessarily conserved, each order is a representative measurement of the input power. This result is especially useful to the proposed approach, since it effectively increases the dynamic range of the sensor. For instance, most black and white CCD arrays provide an 8-bit intensity word; thus once the zero order has saturated, an adjoining order can be used to measure the power and effectively increase the output word to 12-bits and higher. For the case illustrated in



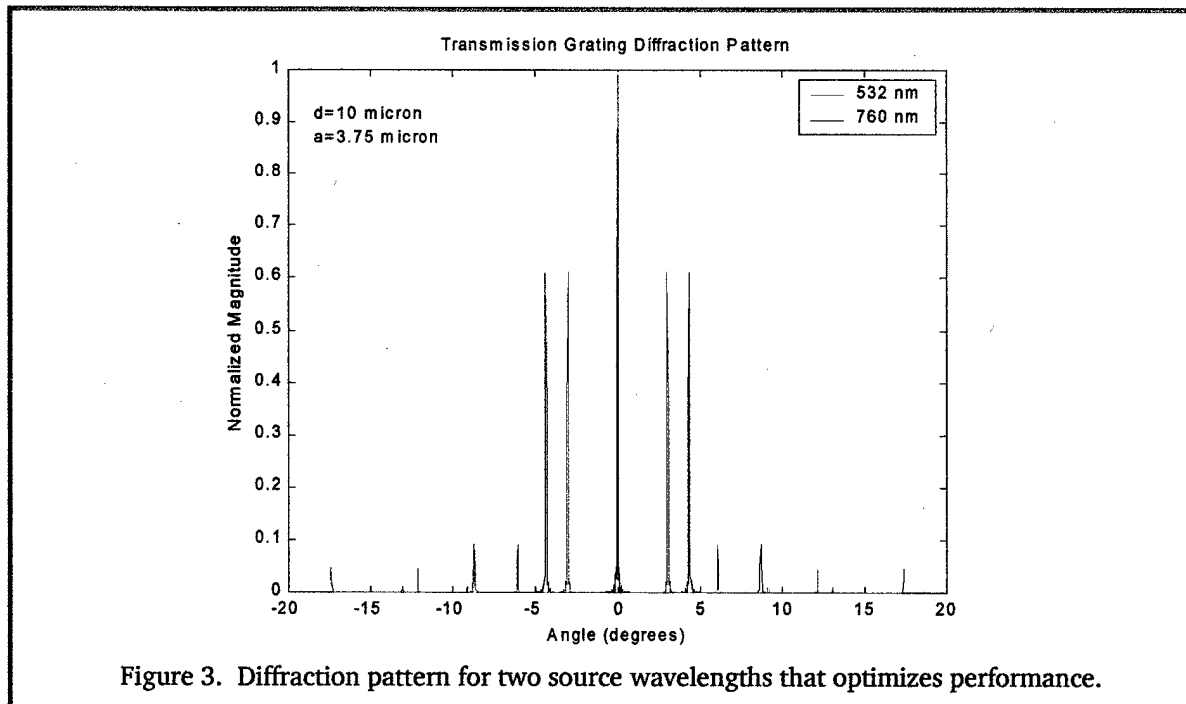
Figure 2, the second order is missing due to the fact that the first zero of the apodization envelope occurs at

$$\frac{\lambda}{a} = \frac{\lambda}{d/2} = 2\lambda/d, \quad (12)$$

which is exactly the same location as the second orders. Thus, by careful selection of the grating pitch and aperture, the order magnitudes can be set to optimize the dynamic range of the system. For instance, by slightly increasing or decreasing the aperture width from one-half of the grating pitch, the second order magnitude can be set to the detection threshold of the system when the first order is saturated, thus realizing a dynamic range of 16-bits, or 1:65000. Finally, this doesn't have any ramifications on the wavelength measurement since power saturation does not effect the spatial relationship between the orders.

Originally, it was believed that the best design approach would be to use a blazed diffraction grating in order to split all the input power between two orders. This idea was mostly brought about due to our traditional experience in designing system that typically dig signals out of noise to optimize performance. However, our analysis and testing throughout the Phase I effort have lead us to the conclusion that in order for the signal to be of any interest (i.e. to reach the glare threshold), the power necessarily will be well above the background. This result coupled with the advantages of increasing the dynamic range by using higher orders has lead to our decision to scrap the use of a blaze angle. Furthermore, this decision is advantageous from a marketing standpoint since it is less costly to fabricate a transmission grating without a special blaze angle.

The key parameters for the grating design are then aperture (size and type) and pitch (aperture repetition period). Figure 3 shows the diffraction pattern for two different wavelength sources after passing through a 10- $\mu\text{m}$  pitch grating with a 3.75- $\mu\text{m}$  clear aperture. These grating parameters were picked based on 1) a 10- $\mu\text{m}$  pitch is an industry standard number, which makes it a low-cost item to manufacture, and 2) a 3.75- $\mu\text{m}$  aperture results in the second order being approximately 90% down from the zero order, which places it at the threshold level when the zero order saturates.



Notice also from Figure 3 that the separation of the orders changes with the wavelength but that the relative magnitude of the orders is unchanged for a given wavelength. This is because envelope function scales with the wavelength (refer to Equation 12). Thus, the detection threshold will not be wavelength dependent, which makes the overall design simpler and the end cost lower.

### 3.1.1 Grating Experimental Results

We used a Canadian Photonics Laboratories CCD camera/grating combination to verify the ability to measure wavelength and intensity of a pair of laser diodes at 640 and 785 nm respectively. Table 2 shows the hardware information of the test setup.

Item	Setting
Camera	Canadian Photonics Laboratories CPL-103MS
CCD type	Interline Transfer
CCD size	640 × 480 pixels
CCD pixel size	8-μm
Image area	5.2 × 3.7 mm
Lens focal length	8-mm
Grating	Optra, Inc.
Type	Holographic transmission
Pitch	20-μm
Aperture width	10-μm
Frame Grabber	Integral Technologies FlashBus MV Lite
Laser diode 1	Phillips Electronics CQL845
Wavelength	640-nm
Laser diode 2	Rohm RLD78MA4
Wavelength	785-nm

Table 2. CCD/Grating analysis breadboard test setup information

Figure 4 shows the Philips laser diode image and Figure 5 shows plot of the intensity for the row with diffracted orders laser compared to the grating model.

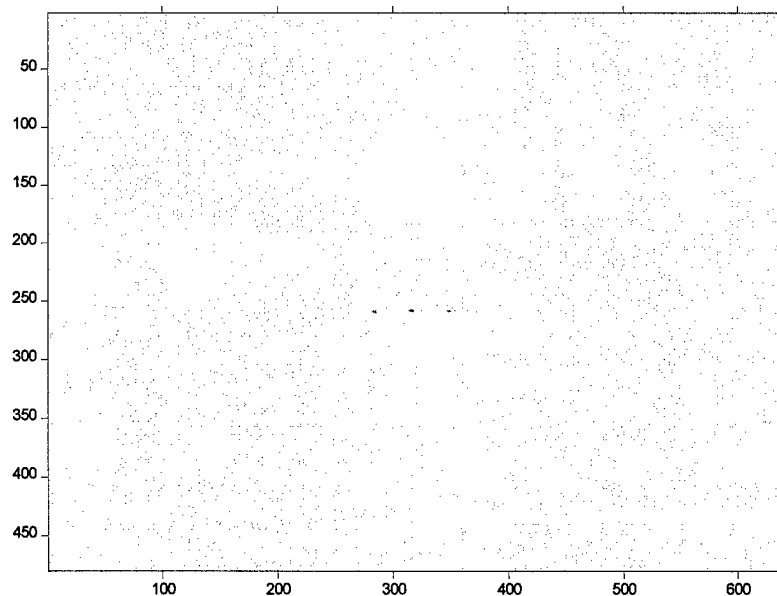


Figure 4. Philips 640-nm laser diode inverted image using the Canadian Photonics CCD camera and 20-μm grating

The image in Figure 4 was inverted in order to present the non-lit background as white rather than black. Note that since the lens focuses the narrow-band laser light onto the array it is difficult to pick out the diffracted orders in the image (because they are effectively focus onto one pixel). However, it is clear from the Figure 5 that light from the diffracted orders is easily discernable above the background, making them easy to detect. The model and the measured data show a good overlay, verifying the ability of the grating to separate the orders in angle by an amount proportional to the wavelength. The width of the orders is somewhat larger than the model due to the point-spread function of lens, indicating that the grating is not limiting the effective resolution of the system, as expected from the analysis. However, a blow-up of the region around the first order plotted in Figure 6 shows that the intensity falls off rapidly, indicating a resolution of one pixel is still achievable, which translates to a wavelength resolution of 20 nm for the present setup. Also, notice that there is not any intensity at the even orders, due to the fact that the duty-cycle of the grating is 50% (Eq. 12). Lastly, notice that the third orders are not visible at this intensity since they are buried in the noise.

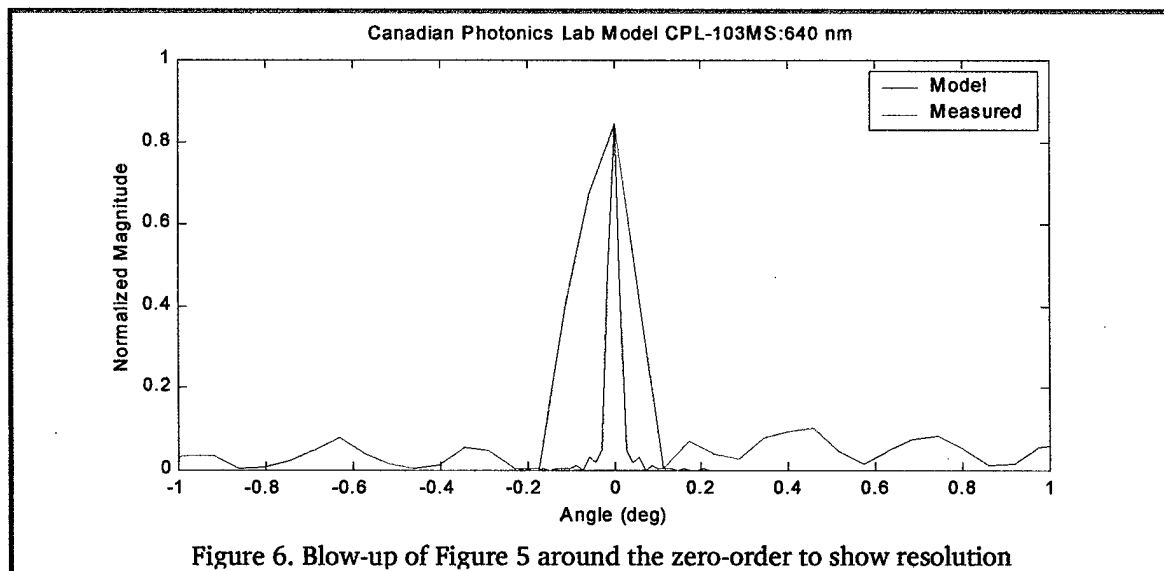
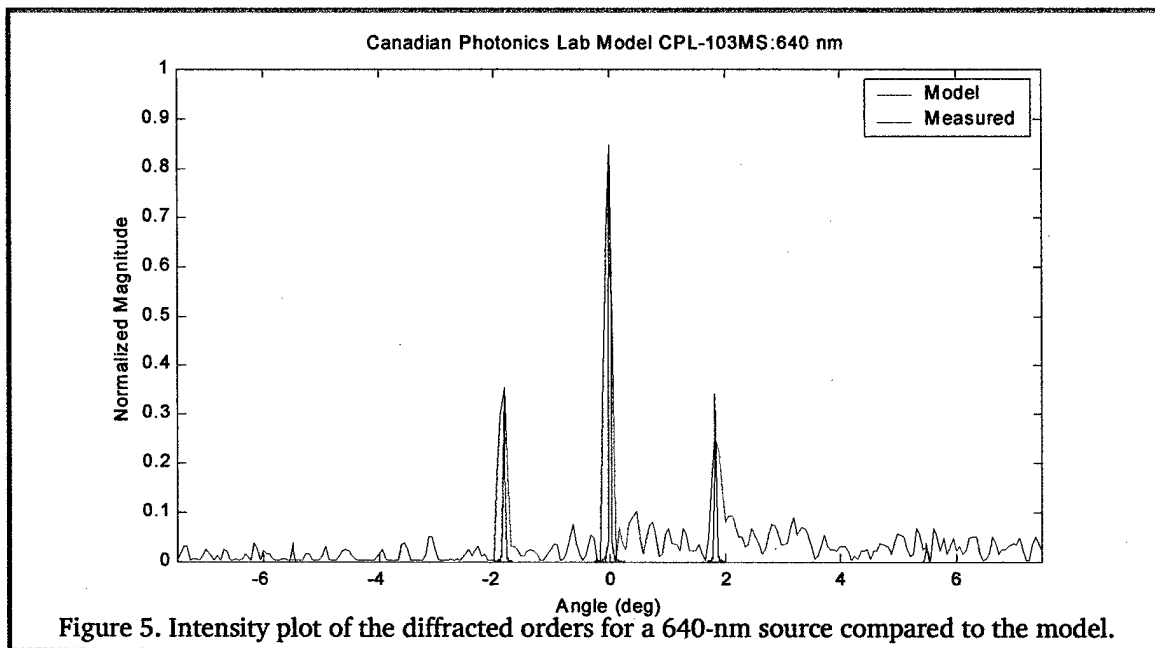
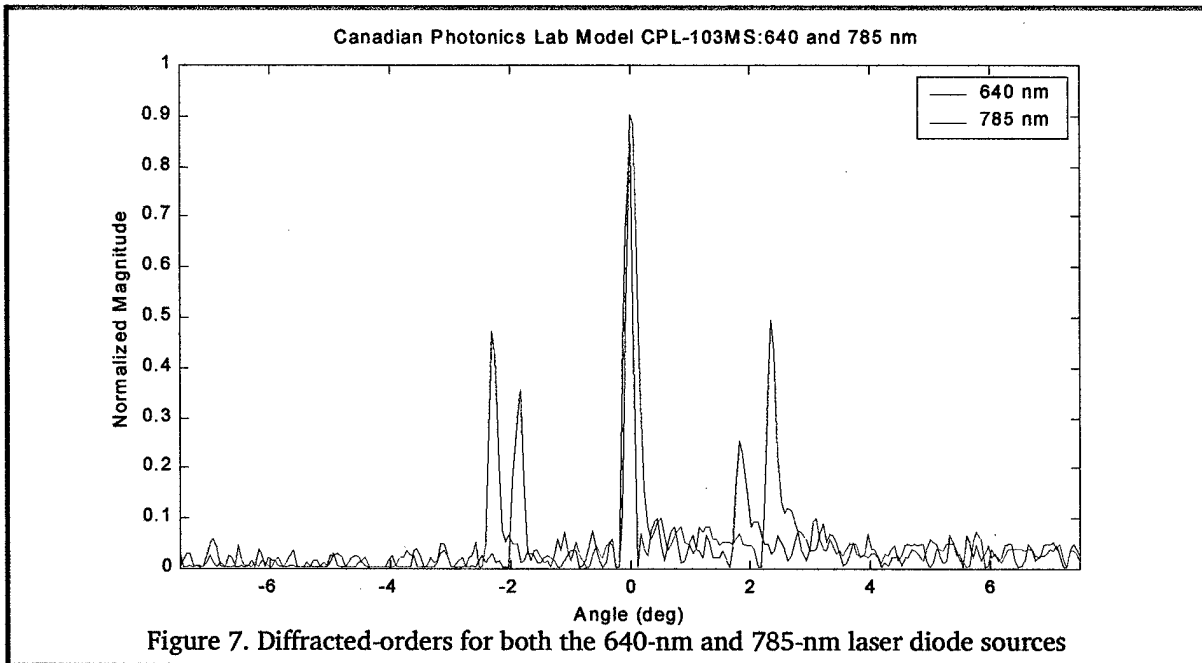
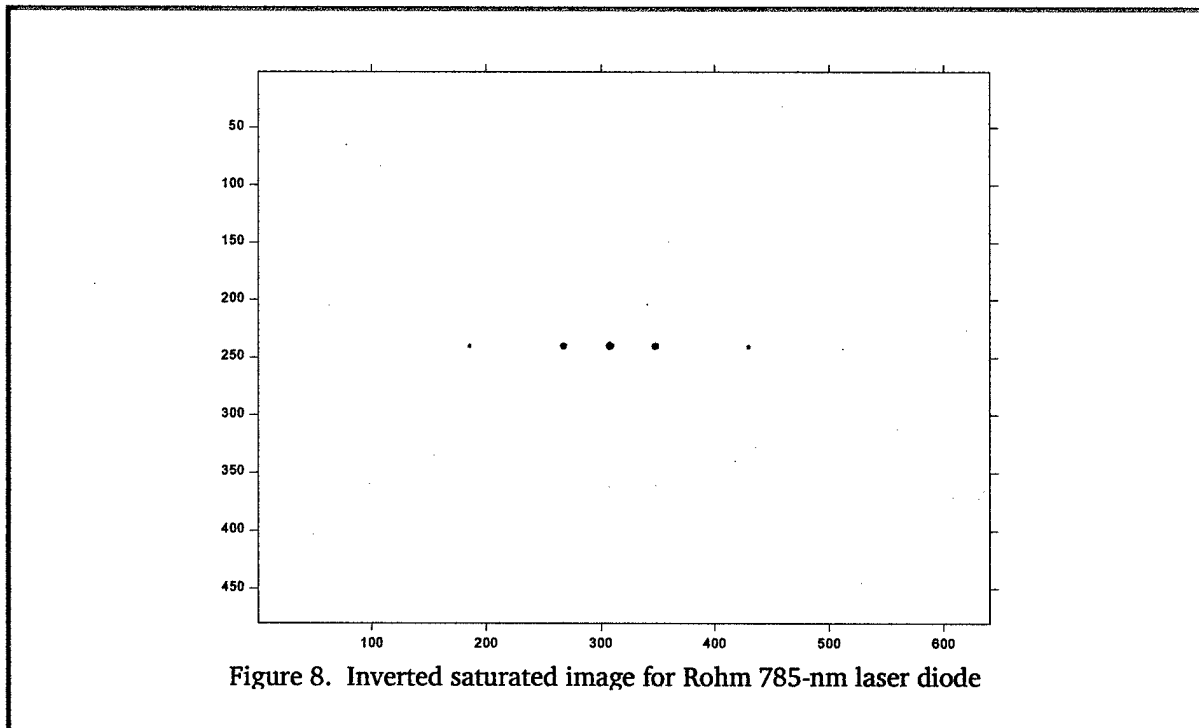
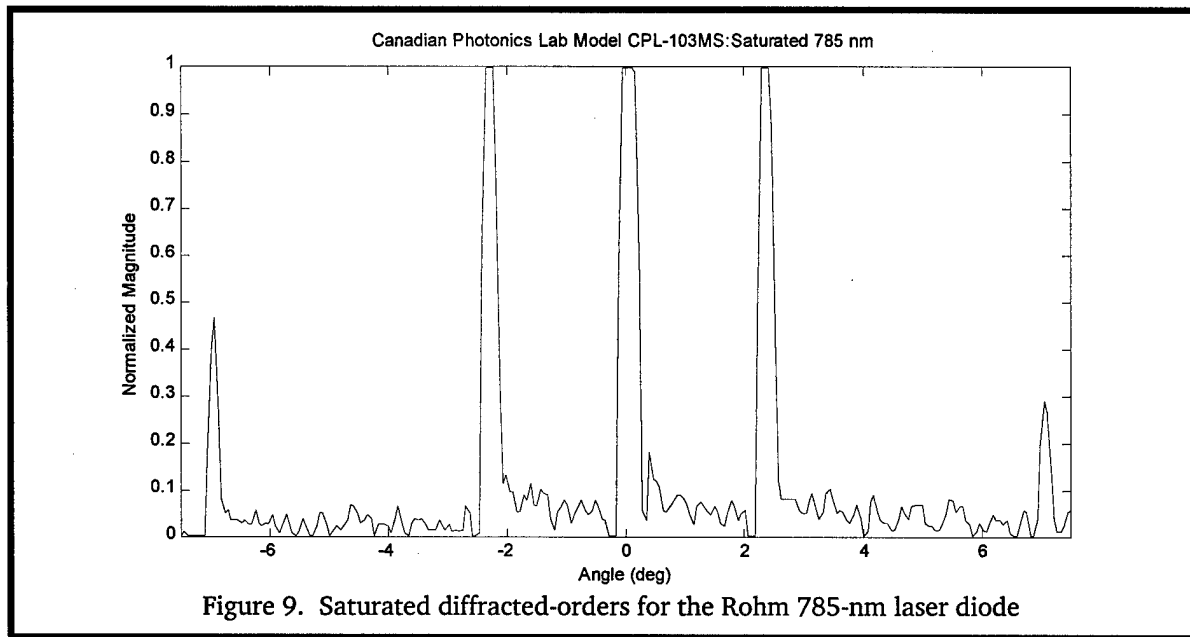


Figure 7 shows a comparison between the diffracted orders for the Philips 640-nm laser diode and the Rohm 785-nm laser diode, clearly indicating that both lasers are easily resolvable.



Finally, Figure 8 shows a image when the laser power is large enough to saturate the image and Figure 9 shows the resulting intensity plot of the diffracted orders. It is clear from the latter figure that even though zero and first orders are saturated, the separation between them remains unchanged and the now-visible third order contains the intensity information. Also note in Figure 8 that saturating the CCD array caused a little smearing, but that it did not have much of an effect on the diffracted orders visibility or width as seen in Figure 9.





### 3.2 Radiometry Analysis

Damage and light-induced stress at the human retina depend on the following:

1. The irradiance level at the retina (which depends on the diameter of the eye pupil);
2. The duration of the exposure;
3. The retinal area exposed; and
4. The wavelength (which determines the extent to which the light is absorbed at the retina).

When laser light damages the retina, particularly in a military situation where the laser source is likely to be at a large distance, the source can generally be regarded as a point source. That is to say, the image area on the retina depends only on the imaging properties of the eye — taking into account factors such as diffraction, chromatic aberration, de-focus of the eye, and other aberrations. We will use  $a_0(\lambda)$  to stand for the diameter of the image spot on the retina when it is illuminated by a point source. This is a function of wavelength,  $\lambda$ , because of the strong chromatic aberration of the human eye. In the visible, on a cloudy day, reasonable values for  $a_0$  and  $D_E$ , the diameter of the eye pupil are  $10\mu\text{m}$  and 2 to 3mm, respectively.

The variables that we will use to describe the radiometric situation are defined in the table below.

SYMBOL	DEFINITION	UNITS
$P_0$	Power emitted by the laser	watts
$N_s$	Radiance of a non-laser source	watt/cm <sup>2</sup> -strd
$H_0$	Irradiance at the plane of the eye	watt/cm <sup>2</sup>
$H_R$	Irradiance at the retina	watt/cm <sup>2</sup>
$T_E(\lambda)$	Transmission of the eye (function of wavelength)	
$D_E$	Diameter of the eye pupil ( $\approx 0.2\text{cm}$ )	cm

SYMBOL	DEFINITION	UNITS
$f_E$	Effective focal length of the eye ( $\approx 1.7\text{cm}$ )	cm
$a_o(\lambda)$	Diameter of the image of a point source on the retina	cm
$A_R(\lambda)$	Fraction of light absorbed at the retina	
$S_o$	Cross-sectional area of the laser beam at the eye	$\text{cm}^2$

The following equations can be used to estimate the retinal irradiance levels for lasers and extended (non-laser) light sources:

Laser source: 
$$H_R = H_o T_E (D_E/a_o)^2 = (P_o T_E/S_o)(D_E/a_o)^2 \quad (13)$$

and,

Extended source: 
$$H_R = N_s T_E (\bullet /4) (D_E/f_E)^2. \quad (14)$$

To convert these quantities to *absorbed* retinal irradiance, one simply multiplies by  $A_R$ . For visible light, the product  $A_R T_E$  has a value on the order of 0.6.<sup>3</sup>

In the plot shown below we have combined a variety of data. The data points that have been plotted represent different light sources. They have been calculated using equations (13) and (14) above, but are in close agreement with similar published data.<sup>4</sup>

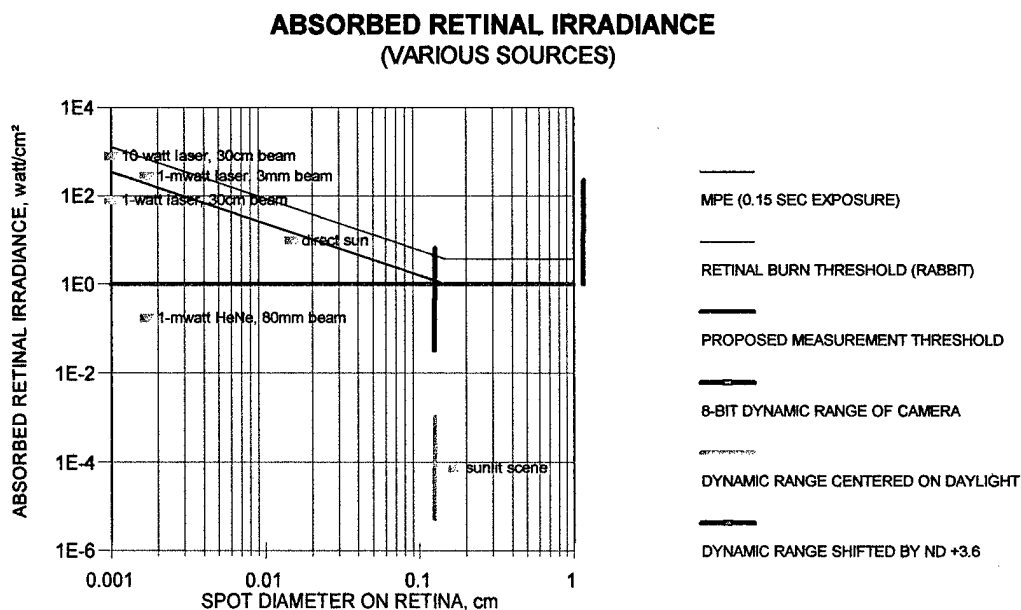


Figure 10. Absorbed retinal irradiance

In this plot the Y-axis is the *absorbed retinal irradiance* (this is the quantity most directly related to retinal damage or stress), and the X-axis is the diameter of the illuminated spot on the retina. The reason that this spot diameter is relevant is that for a small retinal image, localized heat can be conducted away by adjacent tissue; for a large spot this is no longer possible except at the

<sup>3</sup> Sliney and Wolbarsht, "Safety with Lasers and other Optical Sources," (Plenum Press, New York, 1990), p.121.

<sup>4</sup> Sliney and Wolbarsht, op.cit., p.135.

edges of the spot. Thus a given irradiance level may be more damaging when it illuminates a larger spot.

The red line on the plot shows the retinal burn threshold for a rabbit's eye (frequently used as a surrogate for a human eye), and the black line shows the Maximum Permissible Exposure (MPE) for a 0.15sec exposure duration (0.15sec is about the time it takes for an eye-brain response to a visual signal). The heavy green line shows what we are proposing for a Measurement Threshold; we will explain what we mean by this in the following paragraphs. The blue vertical line shows the dynamic range of a standard black-and-white digital video or still camera (8-bits, or 256 gray levels). Within this range, one can make linear measurements of irradiance.; at higher light levels the signals will be saturated, and at lower levels the signals will be in the noise (less than an LSB).

In radiometric terms, the laser warning detection problem comes down to locating the dynamic range of the detector (digital video camera) so that it is sensitive to laser threats of interest. The location of the 8-bit dynamic range of the detector on the vertical axis in figure 1 above can be easily adjusted by the use of an ND (neutral density) filter in front of the camera. In order to demonstrate this in relevant terms, we carried out the following demonstration.

### 3.2.1 Radiometry experimental data

We used a digital camera whose exposure was set to record a brightly lit daylight scene. Included in the scene was a 1 mwatt HeNe laser aimed at the camera, and having a beam diameter of about 8 cm at the camera ( $H_0 \approx 2 \times 10^{-5}$  watt/cm<sup>2</sup>;  $A_R H_R \approx 0.5$  watt/cm<sup>2</sup>). This light source is shown in figure 10 as a purple square labeled "1 mwatt HeNe, 80mm beam." It is well below the MPE level for a 0.15sec exposure duration, and just below the proposed threshold exposure level (heavy green line). In fact, when viewed directly this laser source was very bright, but not painfully so — and there was no noticeable after-image (an indication of retinal saturation and a warning that a dangerously high light level is being approached). Figure 11 shows this scene as recorded by a digital camera whose exposure was set to accommodate the scene. The estimated location of the camera's dynamic range is shown by the orange vertical bar in figure 10. Note that the laser level is above the upper end of this bar, indicating that the image of the laser should be saturated — as it is (note that the center of the laser image is yellow, not red).

The same scene was then recorded with a linear grating and an ND+3 filter in front of the camera. The grating has a transmission of  $\approx 50\%$  (ND+0.3), and the distribution of diffracted light into the various orders is roughly equivalent to an additional 50% attenuation of the irradiance of the zero-order image in the image plane. Thus the net attenuating effect of the grating and ND+3 filter is roughly equivalent to an ND+3.6 filter. In view of this, the dynamic range of the filtered camera is moved up in figure 1 by an amount 1E3.6, as shown by the red vertical bar. We expected that this would result in an image in which the daylight scene was below the detectable threshold and the image of the laser would be at the low end of the dynamic range of the camera+filter. Figure 12 shows this image (converted to gray scale and inverted so as to give a gray image of a small source on a white background), and indeed the daylight scene is below threshold, and the laser image is at the low end of the image's dynamic range. Figure 13 shows an enlargement of the diffracted laser images, and figure 14 shows an image of the sun obtained under the same exposure conditions. Note how the separation of the diffracted images of the laser source line up with the red portion of the diffracted images of the sun. Note also that the sun's zero-order image (the one in the center) is probably saturated, as would be expected from the data in figure 10.



**Figure 11. Sunlit scene with HeNe laser**

The 1.2mwatt HeNe laser was reflected by a spherical mirror to give a 5cm diameter spot at the camera location. The photograph established the baseline exposure (aperture and exposure time) for all of the pictures on this page.

All of the pictures shown here were obtained with a digital color camera (1024 x 768 pixels).

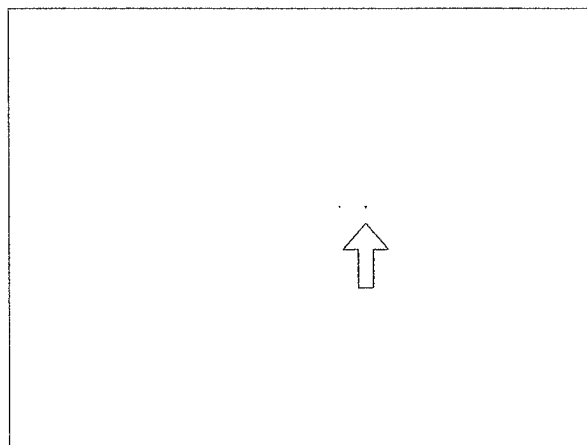


**Figure 12. Sunlit scene with grating & filter**

In this photograph, a diffraction grating and ND 3.0 filter (1000X) were inserted in front of the camera lens and the same exposure as above was used. To print this photograph, the image was converted to gray-scale, adjustments were made to the brightness and contrast, and the image was inverted to avoid printing a large expanse of black. Note that the effect of the filter has been to eliminate everything except the laser. (The arrow points to the zero-order image of the laser source.)

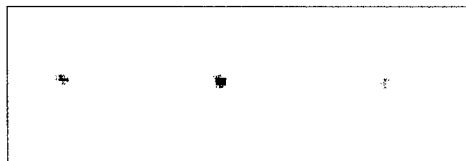


**Figure 13. Sunlit scene with grating & filter**

Same as above with 6X magnification showing individual pixels.



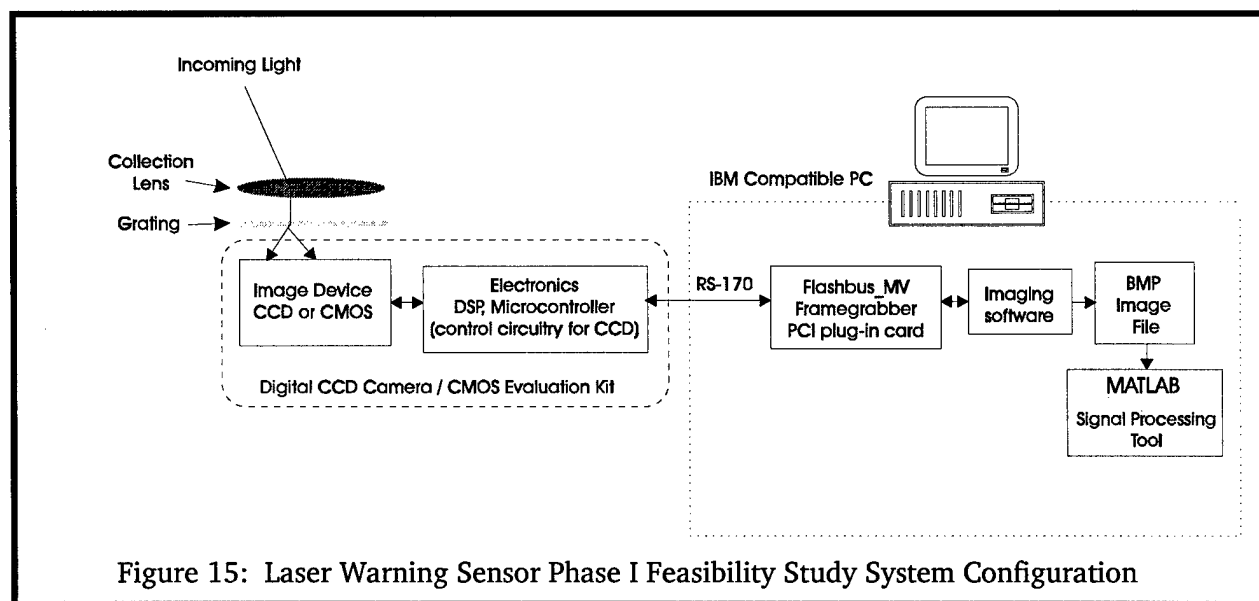
**Figure 14. Direct view of the sun**

Same magnification and exposure as photo above, showing a direct view of the sun. Note the spectral dispersion in the  $\pm 1$ -order images.



### 3.3 Image Sensor Research

The Laser Warning Sensor System Configuration for the Phase I feasibility study is shown in figure 15. Incoming light collected from an input lens is diffracted into multiple order with a diffraction grating. The diffracted orders are imaged, along with a background scene onto an imaging sensor array. The image is transferred, via RS-170 video signal, to a FlashbusMV Lite framegrabber PCI board resident in an IBM compatible PC. . The RS-170 is an 8-bit composite signal that can be input directly into an analog-to-digital converter, which represents the cleanest way to acquire our video signal. The introduction of color would add additional pre-digitized decoding circuitry that would degrade the clarity of the video signal. Imaging software displays the scene live on the PC monitor during breadboard alignment and integration. Single image frames are collected and stored in uncompressed Windows Bitmap (BMP) files for digital post processing. BMP is an uncompressed coded representation of the video scene. An 8 bit Bitmap has a maximum of 256 colors (gray scale) and each pixel in the bitmap is represented by a 1-byte index into the color table. Each bitmap file contains a bitmap-file header, a bitmap-information color table, and an array of bytes that defines the bitmap bits (intensity level of each pixel). MATLAB digital signal processing toolbox is used to process and analyze the image data while Corel Photo-Paint software is used to investigate and display the image quality of the Phase I evaluation devices.



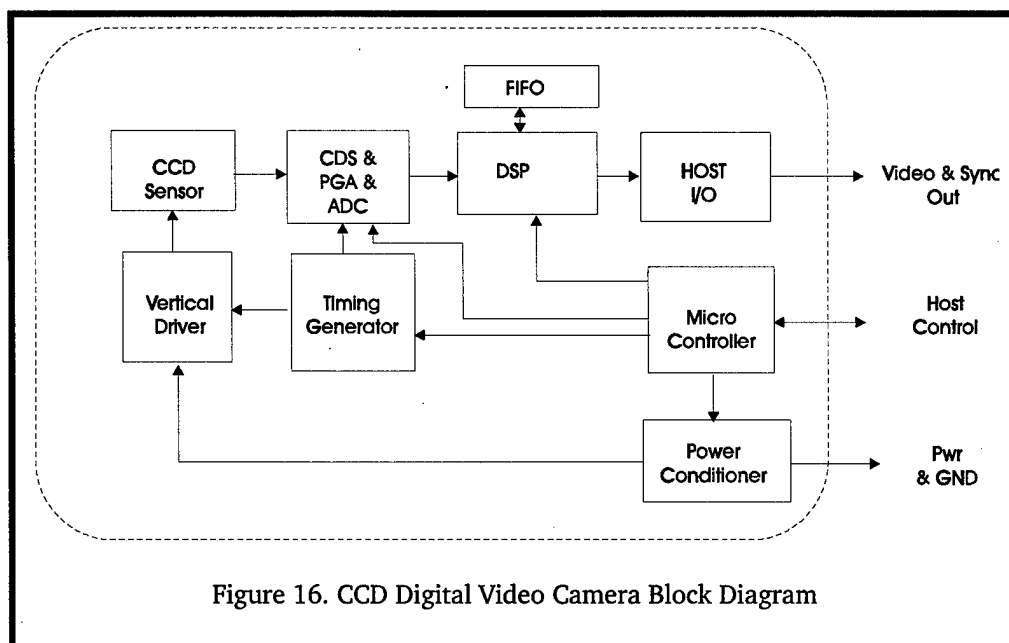
Two imaging sensor technologies have been investigated in the Phase I effort, namely CCD (charged coupled device) and CMOS (complementary metal-oxide semiconductor). The merits by which the imaging device will ultimately be chosen will include: radiometric sensitivity, resolution, responsivity (spectral dynamic range), size (spatial dynamic range) as well as image smear (temporal based image smear), noise, and blooming (spatial image smear due to charge overflow). Six image sensors, as listed in Table 3, were procured and evaluated in the Phase I effort.

Device	Type	Resolution	Mfg	Array Size
CPL-103A7E	CCD – IT	8 $\mu\text{m}$ sqr <sup>5</sup>	Canadian Photonics	640 x 480
CPL-103A7C	CCD – IT	8 $\mu\text{m}$ sqr	Canadian Photonics	640 x 480
CPL-103MS	CCD – IT	8 $\mu\text{m}$ sqr	Canadian Photonics	640 x 480
CPL-C20A380	CMOS	13.6 $\mu\text{m}$ sqr	Canadian Photonics	512 X 492
OV7010AA	CMOS	8.4 $\mu\text{m}$ sqr	Omnivision	628 x 582
D-500L	CCD – IT	NA <sup>6</sup>	Olympus	1024 x 768

Table 3: Image Sensors Investigated in the Phase I Feasibility Study

### 3.3.1 CCD Image Sensors

Figure 16 shows a typical CCD-based digital video camera. The CCD image sensor primarily works as a light-to-voltage converter. The CCD array requires complete electrical support in order to deliver a stream of digital bytes to represent the light collected at each pixel. A timing generator creates a complex set of timing signals to collect, transfer, and shift the analog voltage values out of the chip. A vertical driver converts the timing signals into logic signals at special voltage levels required by the CCD. The output is sent to a Correlated Double-Sampling (CDS) chip which subtracts the background signal from measured signal, which is then amplified by a Programmable Gain Amplifier (PGA) and sent onto the digital to analog converter (ADC).



CCD imaging is performed in a three step process: (1) exposure converts photons of lights into an electrical charge at discrete sites called pixels, (2) charge transfer which moves the packets of

<sup>5</sup> Calculated. Information not available from vendor at this time.

<sup>6</sup> Information was not available from vendor.

charge within the silicon substrate and (3) charge to voltage conversion and output amplification. The architecture of the CCD defines the percentage of photosensitive area, pixel size as well as speed (charge transfer rates). CCD arrays can be classified by (a) architecture (how the stored charge is transferred, thereby defining active pixel area), (b) the quantum efficiency of the device (particularly in the UV spectrum) and (c) the quality, or grade, of the device, specifically, the quantity and layout of "stuck" pixels.

#### *Architecture:*

The bulk of CCD arrays in use today<sup>7</sup> are Full-Frame Transfer and Frame Transfer devices, which use MOS photocapacitors as detectors, and Interline Transfer devices, which use photodiodes as the detector. Full Frame (FF) CCD arrays have the simplest architecture and are the easiest and cheapest to fabricate. The device takes the scene information and partitions the image into discrete elements (pixels) and then shifts the resulting rows of information in a parallel fashion through a shift register resulting in a serial output. This type of CCD array has no 'dead zone' (areas on the chip that are not sensitive to light). Because the parallel register is used for both scene detection and readout, a mechanical shutter or synchronized strobe illumination must be used. This makes the FF CCD array very unattractive. Frame-Transfer (FT) CCD arrays incorporate a storage array that is not light sensitive. The captured scene is shifted from the photosensitive, or image array, very quickly to the adjacent storage array. Readout off the chip is performed while the array is integrating the next frame. The advantage of this architecture is that a continuous (or shutterless) operation is achieved, ultimately resulting in faster frame rates with no moving parts. The resulting performance is compromised by lower resolutions and higher production costs resulting from the need to house both the active area and the storage area in close proximity on the silicon. In Interline Transfer (IL) CCD arrays, the photo-detecting and readout functions are separated by forming isolated photosensitive regions in between lines of the non-sensitive or light shielded parallel readout CCD arrays. After integrating a scene, the signal collected in every pixel is transferred, all at once, into a light-shielded parallel CCD array. Transfer to the output is carried out like FF and FT CCD arrays. During readout, the next frame is being integrated thus achieving continuous operation and higher frame rates, however, their complexity leads to higher unit costs and lower sensitivity. Lower sensitivity occurs because less photosensitive area is present at each pixel site due to the associated light shielded readout CCD array.

#### *Quantum Efficiency:*

In general, the photosensitive area of a CCD is completely covered with polysilicon gates for charge transportation. A front-illuminated CCD device has no response in the UV spectrum because the polysilicon gates absorb the input light. Absorption losses also occur in the visible spectrum resulting in low quantum efficiencies (on the order of 40%)<sup>8</sup>. By flipping the CCD chip over and etching the back surface, absorption losses are avoided. The photo-generated carriers are collected in the bulk silicon and transported via polysilicon gates. This is called a back-thinned, or black lit, device. This results in a device with QE in the 250 nm range on the order of 75% and 90% at 650 nm.

#### *Quality (grade):*

---

<sup>7</sup> *Charge-Coupled Device (CCD) Image Sensors*, Kodak CCD Primer, #KCP-001, Eastman Kodak Company – Microelectronics Technology Division, Rochester, NY.

<sup>8</sup> *Myths about PMTs*, Hamamatsu Corp., Bridgewater, NJ, <http://fiberoptic.com/form3.cfm?VendorID=455>

Each manufacturer specifies grade somewhat uniquely, with exception to the defect free (or zero grade). Grade 1 can also be called 'engineering grade' but the basic concept remains the same. Grade 0 is a perfectly working CCD where every pixel is fully operational. Grade 1 typically allows a certain number of pixel to be stuck (either permanently on or off), typically no more than 10, and typically they are not allowed to be in a single row or form a cluster. Grade 2 usually allows many more, or perhaps an unspecified number of dead pixels, and a finite number of clusters or columns to be dead.

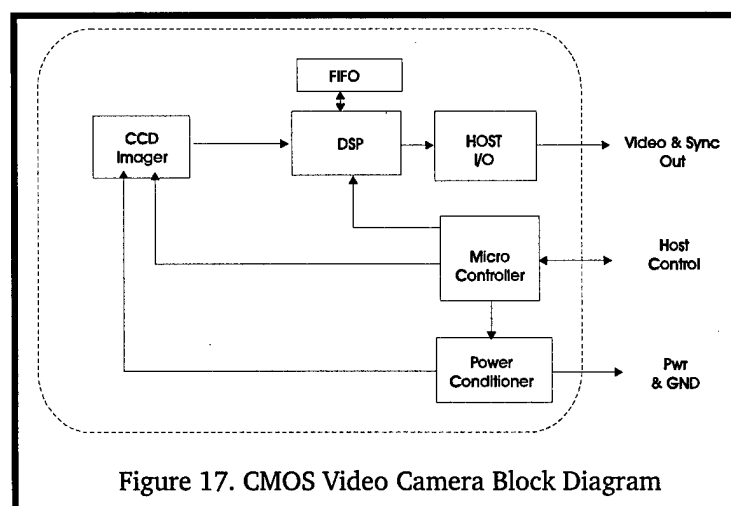
#### *Blooming:*

CCD sensors store photo-generated charges in potential wells isolated from one another by potential barriers. In the event a pixel is saturated by a strong source, the potential well will overflow into a neighbor, thereby blurring or blooming the image. This phenomenon can be reduced by purchasing a CCD image sensor with VOD (vertical overflow drain) or a LOD (lateral overflow drain). Disadvantages to these structures are added complexity and hence increased device cost.

The advantages of using a CCD image sensor include high light sensitivity, good linear response over the device spectrum, and little to no image smear. The disadvantages to a CCD image sensor include complex circuitry to drive, control and receive output from the sensor, multiple voltage sources, high power consumption, as well as high cost. The advantage to competing CMOS sensors for the CCD market has produced much lower cost CCD image sensors being made available.

#### 3.3.2 CMOS Image Sensor

Figure 17 shows a typical CMOS video camera block diagram. A CMOS image sensor is essentially a two-dimensional addressable array of pixels that are selected a row at a time by row address logic. A pixel can consist only of a photodiode and an access transistor (called a 'passive pixel') or with an additional active amplifier integrated within each pixel (called an 'active' pixel). The CMOS image sensor can greatly simplify the imaging system by replacing the vertical driver, timing generator, and CDS/PGA/ADC chips with a single chip. Great strides have been made in producing CMOS image sensors. A  $3.7 \times 3.7\text{-}\mu\text{m}$  pixel size has been recently announced.<sup>9</sup>



<sup>9</sup> H. Ihara, H. Yamashita, I. Inoue, T. Yamaguchi, N. Nakamura, and H. Nozaki, "A  $3.7 \times 3.7\text{-}\mu\text{m}^2$  square pixel CMOS image sensor for digital still camera applications", IEEE ISSCC Digest of Tech. Papers, pp. 182-183, 1998.

Image smear is a common problem with CMOS image sensors. The nature of the CMOS sensor allows a row of pixels to be read out as another row of pixel is integrating an image. The entire image is not integrated in parallel. It is very possible that the scene that was imaged in row 1 has changed before the last row has completed.

The advantages of a CMOS image sensor include integrated timing and control, clock drivers, and analog-to-digital conversion, low power requirement (3.3 – 5 V supply), low power consumption, low cost (\$5 - \$25 per chip in quantities of 1), as well as the non-direct readout architecture of this sensor allows fully random accessibility which enables sub-sampling the image data and higher sampling rates. The disadvantages of using a CMOS image sensor are include image smear and fixed pattern noise – in other words – each pixel has its own amplifier, and variations of the amplifier gain result in a static pattern noise in the background of the image. This may have been evident in the Phase I evaluation devices. However, the incorporation of correlated double sampling has been effective in reducing the amplifier offset related FPN to 0.15 – 0.5%.<sup>10,11</sup>

### 3.3.3 Image Sensor Data

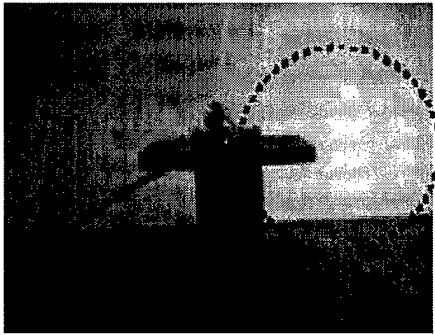
Figure 18 shows data generated from four image sensors. All four photographs are the image of an identical test scene using a 785-nm laser diode beam with an 8-mm focal length lens. Figure 18a and 18b show images taken with two CMOS image sensors with automatic gain and exposure control. The background of the scene was illuminated to create a fast electronic shutter speed. The images are focused on the laser beam spot and not the breadboard hardware. The point of concern on the CMOS sensor images (a and b) is the spatial background intensity variation. This suggests a variation in the pixel-to-pixel gain. It is important for the image sensor to maintain a consistent responsivity throughout the detector array. Figure 18b does exhibit some spatial responsivity variation, however, the results are hopeful. CMOS imaging technology is developing at such an advanced pace it would be premature to rule out their possible use in a Phase II prototype system. The CCD image sensors exhibit uniform gain over the entire field as well as the ability to clearly identify the laser beam spot.

Figure 19 shows enlarged images of Figure 18 in order to show the quality of the image of the focused laser beam. It is imperative that the image detector be capable of containing a high energy spot image within a few pixels without bleeding charge into adjacent pixels. This data shows very promising results. Figure 5c and d (the manual exposure CCD image sensor) as well as Figure 5a (the CMOS image sensor) produce the highest quality laser image. This data clearly demonstrates the ability of low cost compact image sensors to successfully contain high energy laser images within fine resolutions. This data leads us to believe that competent CMOS and CCD image sensors are commercially available with capable spectral response and resolution. The CCD image sensors exhibit more than adequate spectral response and linearity as well. Although the CMOS image sensors are not quite adequate yet, OPTRA will continue to investigate new models and improvements in CMOS imaging technology into the Phase II prototype effort due to these encouraging results.

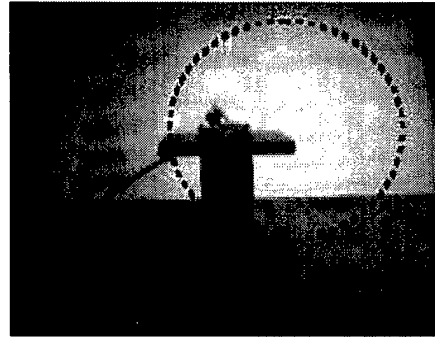
---

<sup>10</sup> R. M., Guidash, T. H. Lee, P. P. K. Lee, D. H. Sackett, C. I. Drowley, M. S. Swenson, L. Arbaugh, R. Hollstein, F. Shapiro, and S. Domer, "A 0.6  $\mu\text{m}$  CMOS pinned photodiode color imager technology", *IEEE IEDM Tech Digest*, pp. 927-929.

<sup>11</sup> R. Nixon, S. E. Kemeny, C. O. Staller, and E. R. Fossum, "128 x 128 CMS photodiode-type active pixel sensor with on-chip timing, control and signal chain electronics", *Charged-Coupled Devices and Optical Sensors III, Proc SPIE*, 1900, pp. 31-39, 1993.



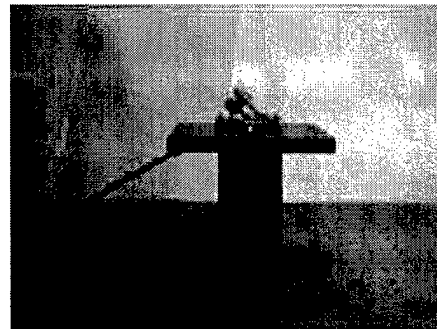
(a) Canadian Photonics  
CPL-G20A380  
CMOS image sensor



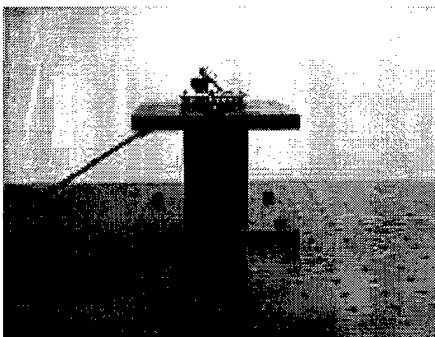
(b) Omnivision OV7010AA  
CMOS image sensor



(c) Canadian Photonics  
CPL-103 MS manu exposure  
CCD image sensor



(d) Same as (c) with higher  
exposure time

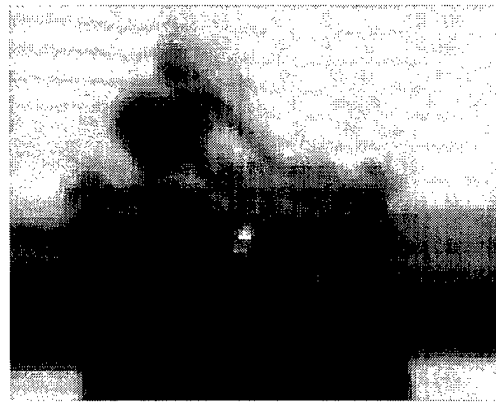


(e) Canadian Photonics  
CPL-103A7C  
CCD image sensor with  
anti-blooming circuitry

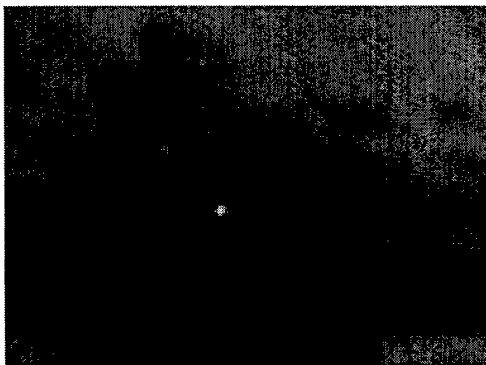
Figure 18: Four image sensors are used to photograph an identical scene of a 780 nm laser diode. The laser diode spot is focused on all image sensors with an 8 mm focal length lens. The background was illuminated with a uniform white light source. The purpose of these images is to show uniform pixel gain across the array as well as anti-blooming control on a slightly saturate laser signal.



(a) Canadian Photonics  
CPL-C20A380  
CMOS image sensor



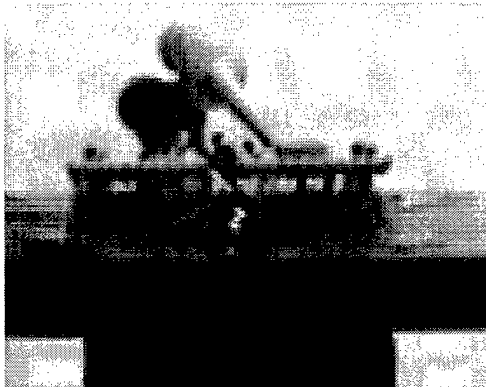
(b) Omnivision OV7010AA  
CMOS image sensor



(c) Canadian Photonics  
CPL-103 MS manu exposure  
CCD image sensor



(d) Same as (c) with higher  
exposure time



(e) Canadian Photonics  
CPL - 103A7C  
CCD image sensor with  
anti-blooming circuitry

Figure 19: The images of Figure 18 are enlarged to show the focused laser beam. Figure 19c and d ( the manual exposure CCD image sensor) as well as Figure 19a (the CMOS image sensor) produce the highest quality laser image. This data clearly demonstrates the ability of low cost compact image sensors to successfully contain high energy laser images within fine resolutions (a few pixel elements) without bleeding charge into adjacent pixels.

Finally, in order to get a sense of the compactness in size that these cameras exhibit, Figure 20 shows a picture of both a CCD and CMOS camera complete with control electronics. Clearly, from this picture alone it becomes very easy to visualize a handheld final product capable of performing all the requisite operations.

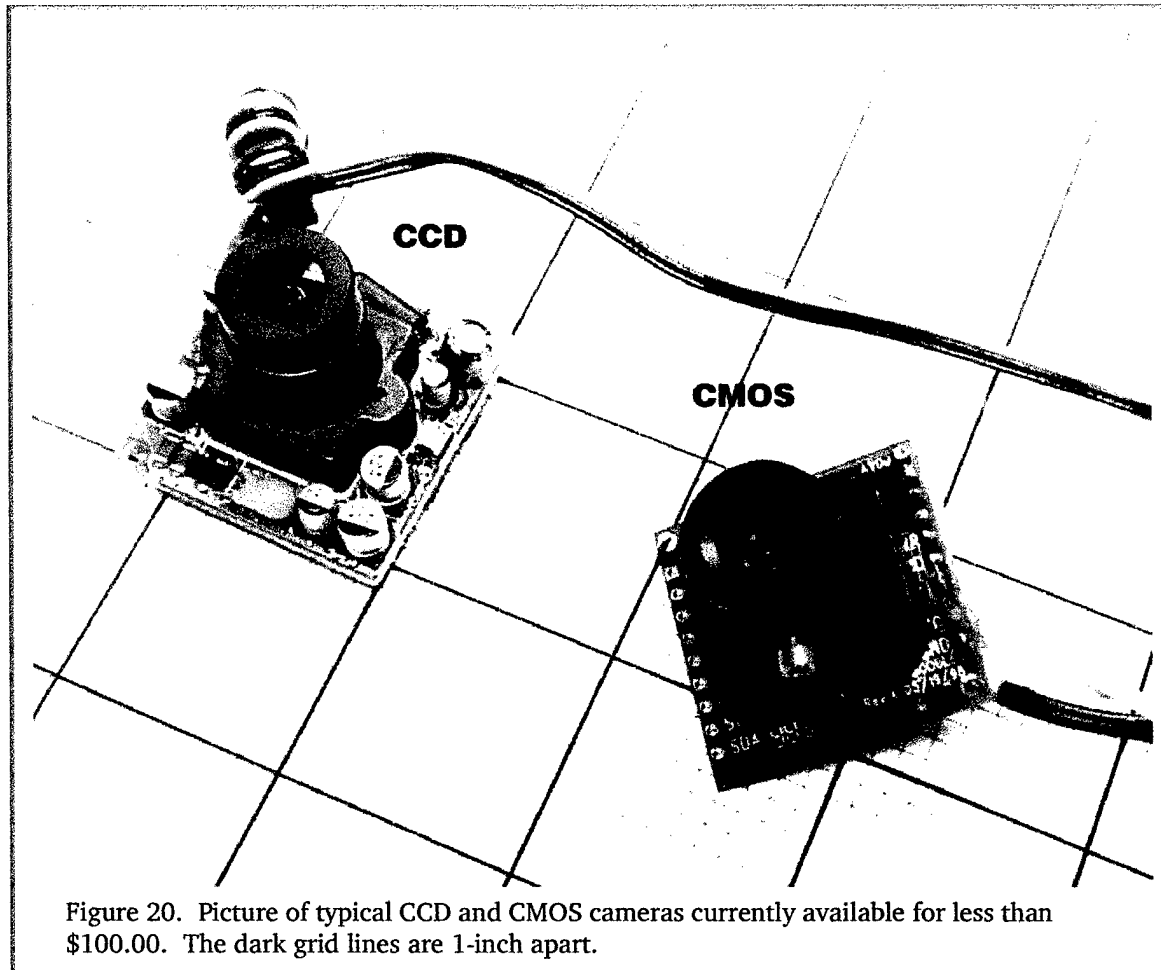


Figure 20. Picture of typical CCD and CMOS cameras currently available for less than \$100.00. The dark grid lines are 1-inch apart.

### 3.4 Cosmic Ray Research

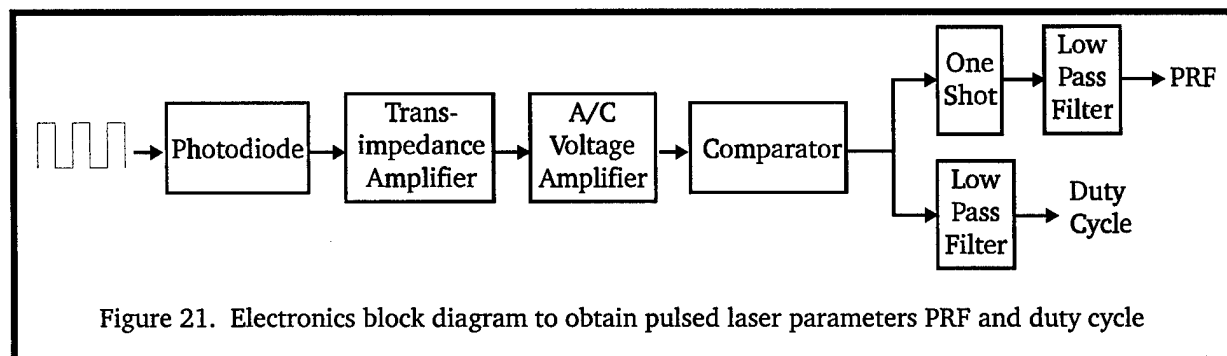
The Phase I feasibility study included research into the possible interference of cosmic rays and how this could be avoided. OPTRA established a contact in the field (Dr. Joachim Rose, an astrophysicist from the Department of Physics and Astronomy at the University of Leeds, Leeds, UK), and discussions were had on possible effects to the sensor from cosmic rays. The outcome of these discussions indicated that a cosmic ray could cause the high-speed photodiode circuitry to mistakenly indicate the presence of a pulsed laser source. However, since the CCD array will now signal the presence of a laser illumination event and then subsequently check the high-speed photodiode for whether the laser illumination is pulsed, cosmic rays are no longer an issue. As a result, no special or extra circuitry will be required in the final product to account for cosmic rays.

### 3.5 Pulsed Laser Detection Electronics

Figure 21 shows a block diagram of the electronics for high-speed detection of laser pulses. The light is sensed with a small area silicon photodiode, which converts the incoming photons to a



current. It is necessary to use a small area photodiode in order to keep the capacitance low and achieve the necessary bandwidth. The photodiode current is then converted to a voltage with the transimpedance pre-amplifier, ac-coupled, and then amplified again with the voltage post-amplifier. A comparator circuit is then used to hard-clip the incoming pulses and generate a train of equal amplitude pulses whose duration is given by the laser pulse length. Two separate circuits are then used to measure PRF and duty cycle, which can then be used to extract the pulse length.



The PRF is obtained by passing the equal amplitude pulse train through a one-shot circuit, which results in a train of pulses that are of equal amplitude and duration, and then low-pass filtering. Since all the pulses into the low-pass filter are of equal amplitude and duration, the low-pass filter, which acts as an integrator, will generate a voltage proportional to the number of pulses over a constant time period, which is proportional to the PRF.

The duty cycle is obtained by passing the equal amplitude pulses directly through a low-pass filter. Similar to the PRF design, the low-pass filter will generate a voltage that is an average of the pulse train. However, in this case the voltage will vary depending on the lengths of the pulses and is thus proportional to the duty cycle. Combining this information with the PRF allows the pulse length to be determined,

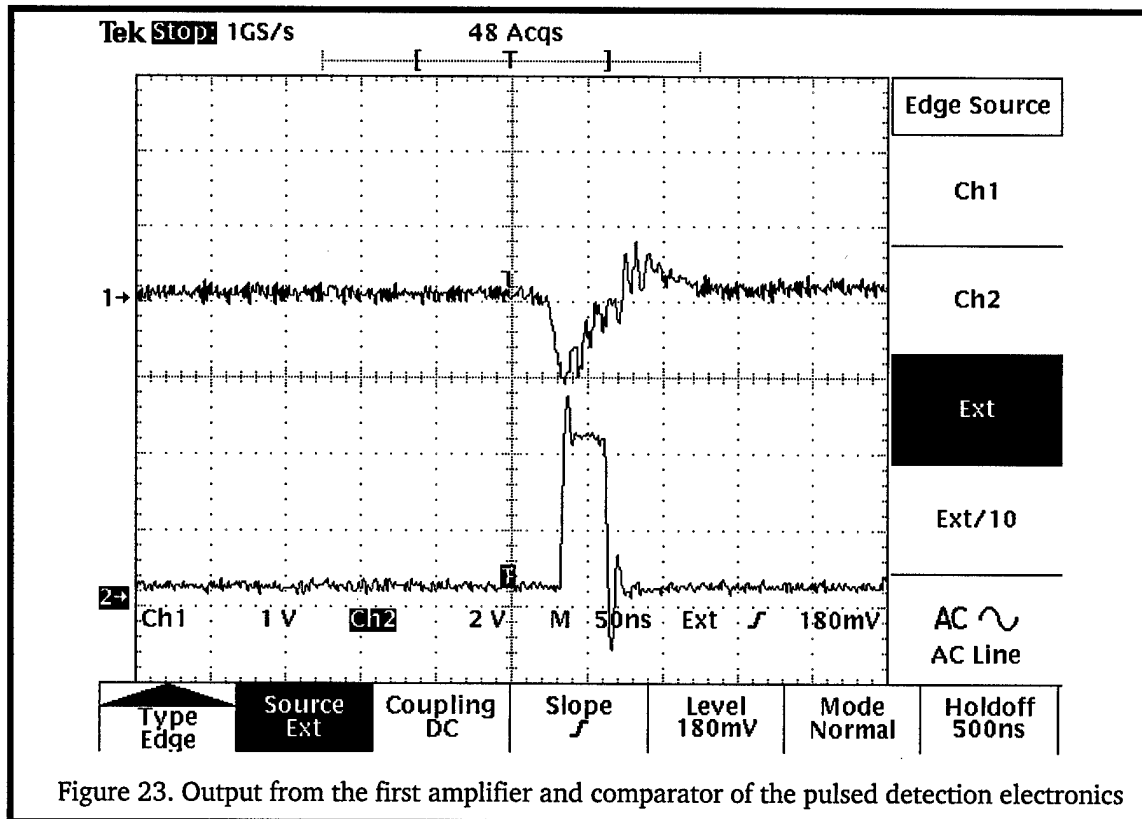
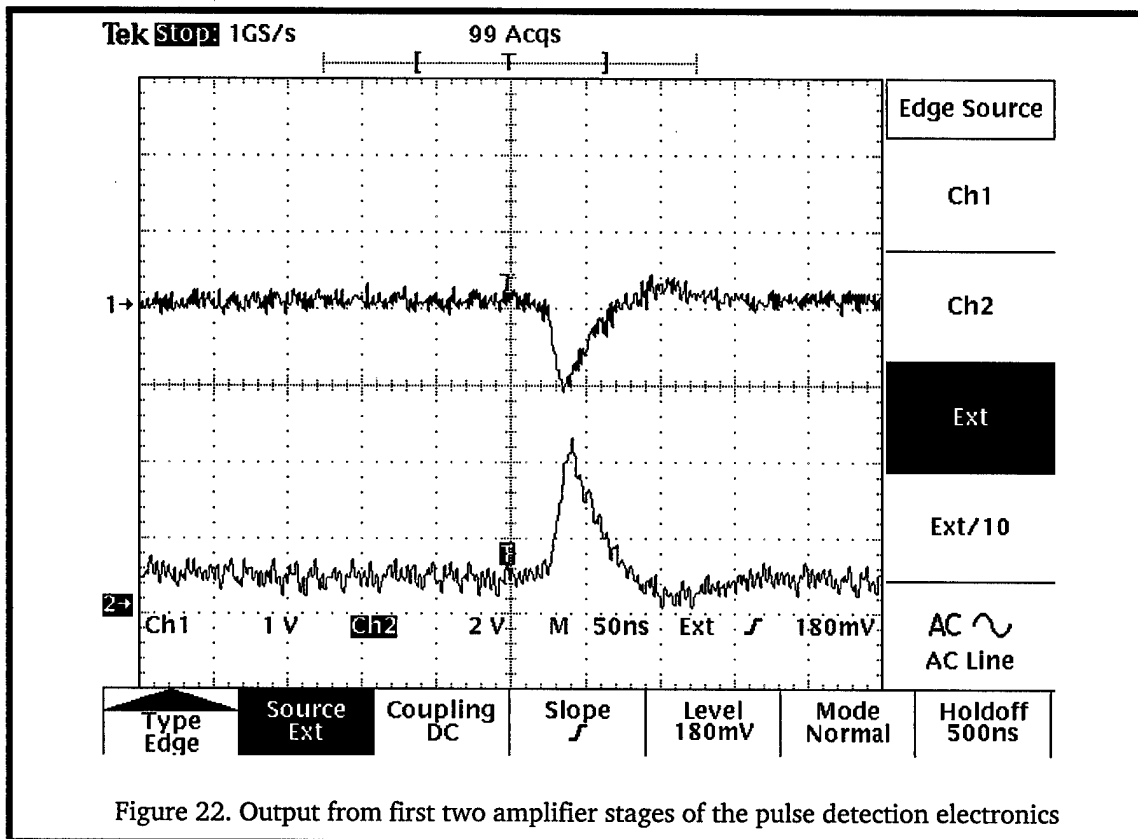
$$\text{Pulse Length} = \frac{\text{Duty Cycle}}{\text{PRF}}. \quad (15)$$

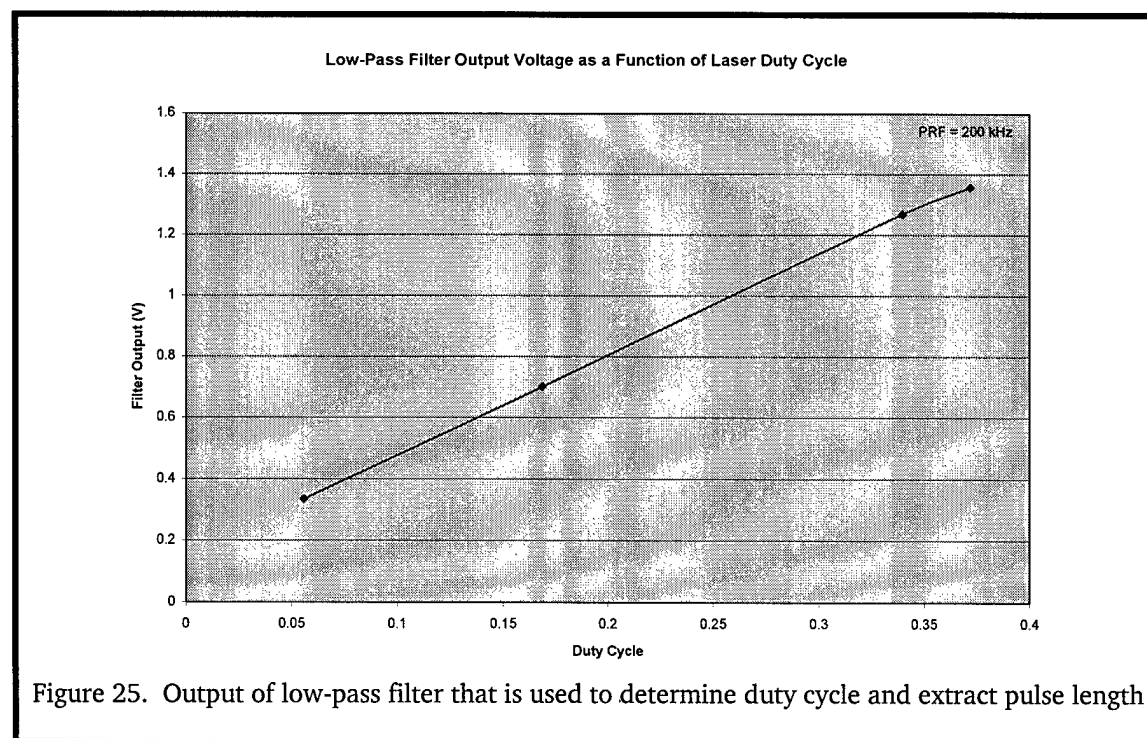
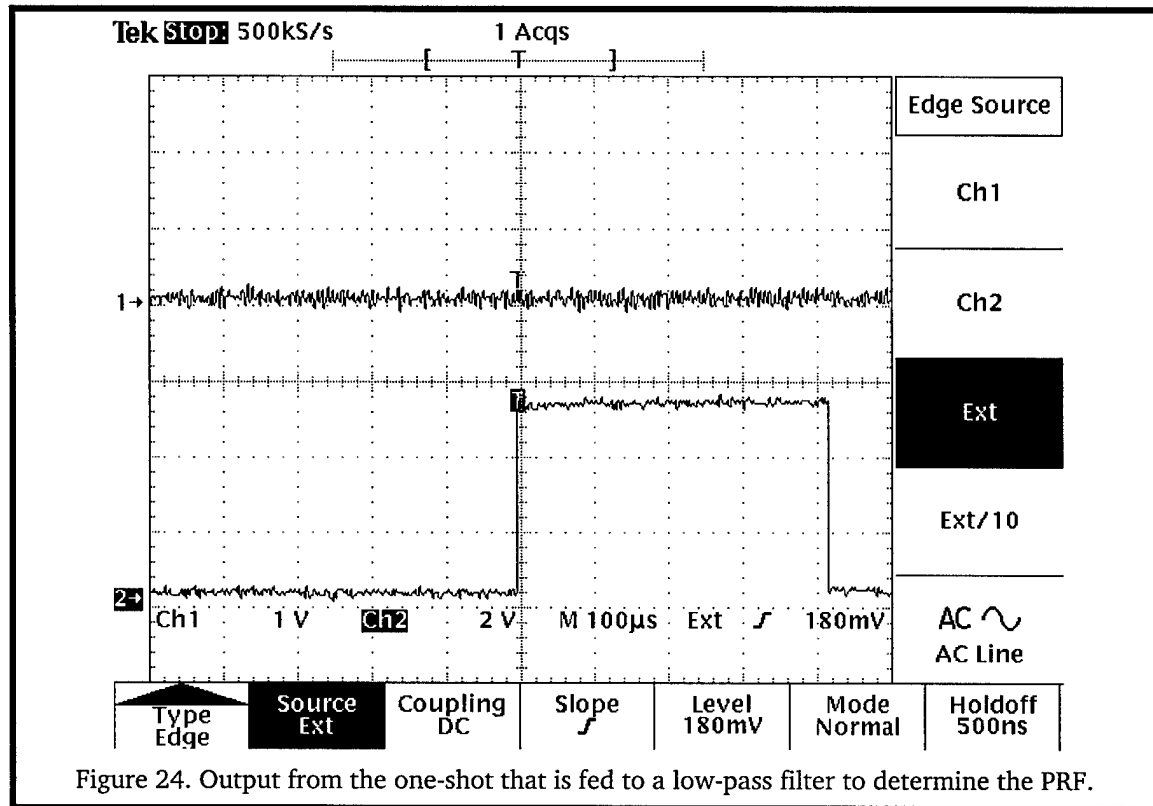
The transimpedance amplifier is a monolithic circuit manufactured by AvanteK, model ITA-12318, which provides a gain of 4000 V/A and a bandwidth of greater than 200 MHz. The voltage amplifier has a gain of 10 V/V and uses a Comlinear CLC425 op-amp.

### 3.5.1 Pulsed Laser Electronics Breadboard Testing

We verified the ability of the high-speed electronics to detect pulses on the order of 50-ns by modulating a 785-nm laser diode and recording the output with a digital oscilloscope. Figure 22 shows the output of the first two amplifier stages, Figure 23 shows the first amplifier output and the comparator output, and Figure 24 shows the output from the one-shot. The output of the one-shot is then passed through a low-pass filter to generate an output proportional to the PRF, which has a scale factor of 2.1 volts/kHz for this design.

Figure 25 shows a plot of the relationship between output voltage and input duty cycle that was obtained by varying the pulse length of a 200 kHz waveform from 250-ns to 1875-ns. This plot clearly shows a linear relationship between the input pulse length and the output voltage. The Phase I testing indicates that with simple circuitry and off-the-shelf components a fairly robust design can be realized that measures pulse lengths on the scale of nano-seconds at a variety of repetition rates.





### 3.6 Algorithm Development

The goal of the image processing is to cleanly extract the laser signal from the background clutter in order to estimate both the laser wavelength and intensity. While the general approach has been identified in the Phase I effort, the majority of the algorithm development and optimization will be done during the Phase II R&D. Effectively, recognition and extraction of the pertinent information will be a two-step process:

- 1) As images are collected in real time, software stored in non-volatile memory will be run with a Digital Signal Processing chip to monitor the serial output that is generated for each frame and determine whether any of the pixels within the image is above a threshold, which is set at a level less than the glare level. Given the positive detection within the image, the image frame and output from the high-speed detector will be time stamped and then transferred to a buffer for event extraction; otherwise, the frame will be deleted to save memory space. Effectively, the purpose of this step is to cull through the data and eliminate those frames that do not have any events. Note that the threshold level will be deliberately set below the glare threshold to allow a certain percentage of false alarms and thereby guarantee that no frames with actual events will be missed. It will be up to the event extraction software to determine which of those frames flagged contain actual laser events.
- 2) Event extraction (e.g. wavelength, power, PRF, and pulse length) will be done on all the images that were flagged by the DSP to contain possible laser sources. Depending on the requirements of the technical monitor as well as the available memory in the DSP, event extraction could be processed real time or post mission after the data has been downloaded to a computer. Regardless of where and when it occurs, a general outline of the procedure for verifying the existence of a laser source and extracting laser event information is summarized by the following:
  1. A temporary image will be created that is equal to the original image, which will be used to manipulate the data and extract the necessary information.
  2. A row vector will be generated that will contain the maximum value pixel in each column along with the location (e.g. row number).
  3. The maximum value of the row vector will then be extracted along with the location (e.g. column). The row and column location from (1) and (2) indicates the location of a possible zero order for the diffracted laser source, since it will be the largest signal within the image.
  4. The magnitude of the candidate zero order signal will be compared to a threshold to ensure that it is not an extraneous signal due to noise.
  5. Next, the location of the candidate zero order signal will be saved to memory and then deleted from the temporary image. The purpose for doing this is that it allows a first order to be found by performing the same set of steps that was used to find the zero order, since it will now be the largest signal within the image. The process continues until a sufficient number of orders and their respective magnitudes have been recovered to determine both the wavelength and irradiance level.
  6. The region around both a candidate first order and zero order signal is examined to determine the spectral bandwidth of the detected source by calculating the full-width, half-maximum of the lineshape (FWHM) and then generating the ratio between the first and zero order signals. What is being looked for is whether the source is truly a laser as opposed to a direct viewing of the sun or glint off a highly reflective object. As can be

seen in Figure 14, the grating causes the diffracted light from a non-laser source to spread in the higher orders (see Equation 7) due to the wavelength dependence of the diffracted angle. Thus, the ratio between the zero and first orders will be one for a laser source and greater than one for a non-laser source.

7. The results for a candidate source magnitude and spectral bandwidth are then compared to magnitude and spectral bandwidth thresholds based on the expected power and spectral linewidth for a laser source – only sources satisfying both criteria will be considered actual laser sources; otherwise, a false alarm will have occurred and processing will cease.
8. The wavelength (from Equation 4) and irradiance level (from Equation 13) are then determined and saved to memory.

### 3.6.1 Algorithm experimental results

During the Phase I effort algorithm development was started in order to extract information from an image that contains a laser source using the steps outlined above. The image processing and algorithm development was performed using The MathWorks MATLAB software and Digital Image Processing toolbox. MATLAB lends itself nicely to the development of the required algorithms since it is based on matrix mathematics, which results in a one-to-one correspondence between a row and column element and the associated pixel within an image. Furthermore, once the algorithms are developed, the MATLAB compiler can be used to convert them to C or C++ code that can then be downloaded into the DSP. This results in a very efficient method of developing code using simple statements and commands already resident within MATLAB, thus bypassing the necessity of doing things twice as well as not getting bogged down in protocol and syntax issues when they are not important to the task at hand. Finally, MATLAB is multi-dimensional in the sense that it will be simple to develop other algorithms so that the proposed sensor can be used in commercial applications of pattern recognition and machine vision.

Figure 26 shows the code from a MATLAB program that was developed to extract the wavelength from the image shown in Figure 12. Plotted in Figure 27 is the row vector containing all the maximum magnitudes for each of the columns after the first time through the image; note that the diffracted orders of the laser are clearly above the background noise. Finally, plotted in Figure 28 is the enhanced image with the results from the MATLAB program for the measured wavelength. Also indicated is the irradiance level for the laser.

```

% This file opens an image of a diffracted laser and
% determines the wavelength
% A major assumption is that only laser energy is
% evident in the image, all others is considered noise

clear

% constants

f = 17.8; % focal length (mm)
d = 0.020; % grating pitch (mm)
w = 12.0; % pixel width (micron)

Io = imread('3-16-base.JPG','jpg'); % Color original image
Ic = imread('3-16-nd3-grat.JPG','jpg'); % Color grating/fltr image
Ig = double(rgb2gray(Ic))/255; % Convert to grayscale

sz = size(Ig); % Image size in pixels

Itmp = Ig; % Temporary image for extracting peaks

for i=1:3 % Just extract 0, 1 orders for now
    [Igm(i),cl(i)] = max(max(Itmp)); % Max magnitude in image
    [Igmxc,rw(i)]=max(Itmp(:,cl(i))); % Row location of max
    Itmp((rw(i)-4):(rw(i)+4),(cl(i)-4):(cl(i)+4)) = 0; % Del peak
end

lmda = (d/f)*(abs(cl(2)-cl(3)))*(w/2)*1000; % Measured wavelength

Ien = imadjust(Ig, [4/255 Igm(1)], [0 1], 0.1); % Enhanced image

% plot figure and label
iptsetpref('ImshowAxesVisible','off')
figure(1), imshow(Io);
title('LWS Data 3-16-98, Unfiltered scene');

iptsetpref('ImshowAxesVisible','on')
figure(2), imshow(1-Ig);
title('ND=3 filter & 20-micron grating');

figure(3), imshow(1-Ien);
title('Processed Image');
text(25,sz(1)-50,['Wavelength: ',num2str(lmda,3),' nm']);
text(550,sz(1)-50,['Irradiance: 2e-05 W/cm^2']); % Power meas

```

Figure 26. MATLAB code to extract wavelength from an image.

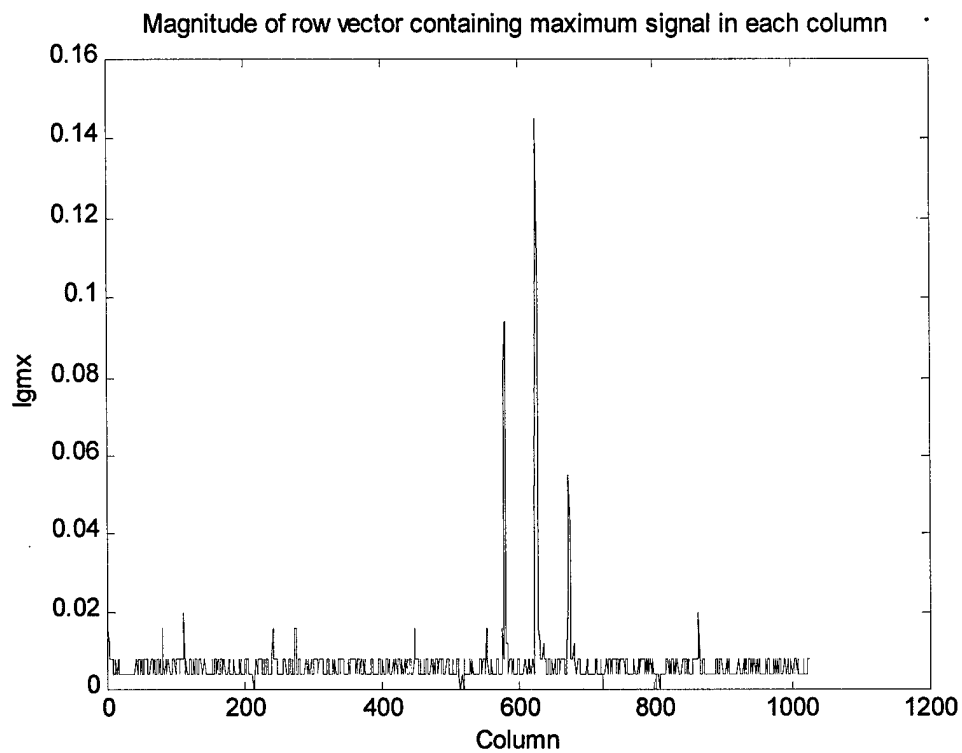


Figure 27. Plot of row vector containing the maximum values for each column

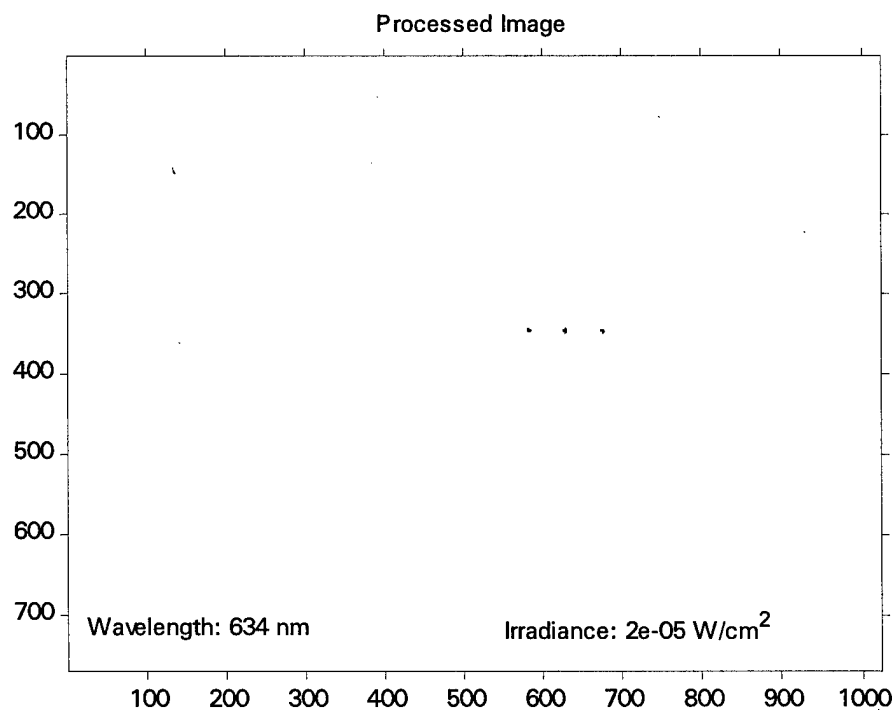


Figure 28. Plot of enhanced image with extracted wavelength and source intensity

#### 4.0 Conclusions

- A grating can be easily realized that separates the incoming laser light into distinct orders whose separation is given by the source wavelength.
- The grating and collection optics will not limit the resolution of the system, which will be set by the pixel width; resolutions better than 10-nm are easily realizable with simple lenses.
- Each of the diffracted orders is in of itself a power meter, allowing the dynamic range to be increased beyond the 8-bits available from the camera to 12- and 16-bits. Thus allows for the achievement of a dynamic range above 1:5000.
- The laser wavelength is coded in terms of the lateral separation of the diffracted images, which can be accurately measured even if the images are saturated.
- Both the CCD and CMOS array sensors are capable of achieving the required spectral response and pixel resolution.
- The CCD sensor appears to do a better job at this point of capturing an image with the minimum level of blooming and smearing.
- The lower cost of the CMOS sensor compared to the CCD array makes it worthwhile for us to continue investigating their performance.
- By using the proper ND filter plus grating in front of the camera, the recorded images contain no sunlit background scene data, and provide images of potential laser threats within the dynamic range of the camera's image. Automated image analysis is greatly simplified by the removal of all extraneous background image data.
- Image analysis will be a two-step process, 1) images will be flagged in real time as possible candidates based on a signal above a set threshold and 2) algorithms will be used to verify the presence of a laser event and then extract pertinent information.
- MATLAB commercial Digital Image Processing software satisfies the required functionality to develop the algorithms necessary to extract event information.
- Cosmic rays will not impact the performance of the proposed system; no special circuitry will be needed.
- The high-speed pulse detection electronics demonstrate the ability to measure and record pulse length and PRF for pulses on the order of 10-ns.
- Nothing in the Phase I research effort has indicated that a final-product that is handheld and costs less than \$500.00 is not possible.

Thus the proposed design appears fully capable of meeting the technical requirements for a Laser Warning Sensor: *it very effectively discriminates against background scene illumination, and can make quantitative measurements of both laser irradiance level and laser wavelength, and laser temporal characteristics.*



## 5.0 Recommendations

### **1. Review of Phase I achievements**

- Demonstration of a filter which, used with a CCD or CMOS camera, allows the recording of potential laser threats from which physical location, irradiance level, and wavelength information can be derived.
- Demonstration of two different 480×640 pixel miniature cameras which are (a) low cost, (b) have 8-bit dynamic ranges, and (c) can fit in a 1-inch cube.
- Demonstration of an algorithm that can be applied to the continuous output from the camera to extract (a) existence of a threatening level of optical irradiance (450nm to 1060nm), (b) location of that threat within the frame, (c) wavelength of the source, (d) spectral bandwidth of the source, and (e) mean irradiance level of the source.
- Development of a non-imaging sensor capable of detecting and recording light pulse duration's and pulse repetition rates of potential laser illumination threats.

### **2. Recommendations for future work**

The Phase I work has, we believe, provided us with all of the critical components needed to develop a small, autonomous sensor for detecting, recording, and analyzing instances of illumination by lasers at irradiance levels high enough to cause visual damage or stress. Future work should focus (1) on assembling these components into a compact, low-power, and inexpensive package and (2) on the development of an optimized means for assessing data collected during a flight, including ancillary data such as date/time, GPS position, etc.

# REPORT DOCUMENTATION PAGE

Form Approved  
OMB No. 0704-0188

Public reporting burden for this collection of information is estimated to average 1 hour per response, including the time for reviewing instructions, searching existing data sources, gathering and maintaining the data needed, and completing and reviewing the collection of information. Send comments regarding this burden estimate or any other aspect of this collection of information, including suggestions for reducing this burden to Washington Headquarters Services, Directorate for Information Operations and Reports, 1215 Jefferson Davis Highway, Suite 1204, Arlington, VA 22202-4302, and to the Office of Management and Budget, Paperwork Reduction Project, Washington, DC 20503

1. AGENCY USE ONLY (Leave blank)		2. REPORT DATE 4/15/99	3. REPORT TYPE AND DATES COVERED Final Report 10/8/98-4/15/99
4. TITLE AND SUBTITLE Low Cost Grating Based Laser Sensor			5. FUNDING NUMBERS N00014-99-M-0008
6. AUTHOR(S) Craig Schwarze, Julie Gargas, Michael Hercher			
7. PERFORMING ORGANIZATION NAME(S) AND ADDRESS(S) OPTRA, Inc. 461 Boston Street Topsfield, MA 01983			8. PERFORMING ORGANIZATION REPORT UNMBER 297
9. SPONSORING/MONITORING AGENCY NAME(S) AND ADDRESSES(S) Office of Naval Research Ballston Tower One 800 North Quincy Street Arlington, VA 22217-5660			10. SPONSORING/MONITORING AGENCY REPORT NUMBER
11. SUPPLEMENTAL NOTES			
12a. DISTRIBUTION / AVAILABILITY STATEMENT Approved for public release; SBIR report , distribution unlimited			12b. DISTRIBUTION CODE
13. ABSTRACT (Maximum 200 words)  The primary objective of this program is to develop a laser warning sensor fo the measurement of laser illumination events during flight at a consumer cost of less than \$500. The target requirements are to measure the wavelength, average power, pulse length, pulse repetition frequency, and duration for each event and save the information in a time-stamped downloadable file. The Phase I effort established the feasibility of the proposed approach by performing a detailed analysis of the design, procuring and fabricating a breadboard prototype, and then performing laboratory testing that soundly verified the ability of the sensor to achieve the target requirements . The sensor has excellent commercial potential in all sectors of the Department of Defense as a laser warning sensor, as well as private sector applications in video surveillance and pattern recognition.			
14. SUBJECT TERMS laser weapons                      high speed detection laser sensor Digital image processing			15. NUMBER OF PAGES 32
16. PRICE CODE			
17. SECURITY CLASSIFICATION OF REPORT                      UNCLASSIFIED			20. LIMITATION OF ABSTRACT UL

April 15, 1999

Office of Naval Research  
Attn: Mr. John Thomas, Code 341  
Ballston Tower One  
800 North Quincy Street  
Arlington, VA 22217-5660

RE: Contract No., N00014-99-M-0008  
SUBJ: Final Report, 0001AD

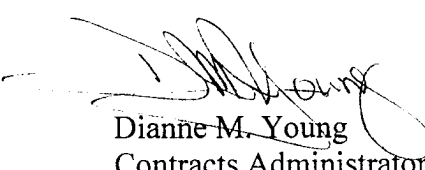
Dear Mr. Thomas,

As required by the above referenced contract, I am forwarding four (4) copies of our final report and a Phase II plan, as requested in ONR letter dated October 30, 1998. I am also enclosing two (2) copies of our DD250. Please sign one copy and forward to DFAS Columbus payment office.

Please feel free to contact me should you have any questions.

Sincerely,

OPTRA, Inc.



Dianne M. Young  
Contracts Administrator

Enclosures

Cc: Mr. Doug Harry, Code 362 (copy of report and DD250)  
DTIC (copy of report)  
NRL, Code 2627 (copy of report)  
DCMC/GFOG Boston, (copy of letter and DD250)  
DCMC/GFOM (copy of report and DD250)  
ONR, Code 253 (Copy of DD250)